University of Nevada, Reno

The Compact Pulsed Power Generator Sparky II and Two X-ray Spectroscopic Devices for Diagnosing Laboratory Plasmas

A thesis submitted in partial fulfillment of the requirements
for the degree of Master of Science in Physics

By

Matthew C. Cooper

Dr. Victor L. Kantsyrev/Thesis Advisor

December 2016

THE GRADUATE SCHOOL

We recommend that the thesis
prepared under our supervision by

MATTHEW C. COOPER

Entitled

The Compact Pulsed Power Generator Sparky II And Two X-Ray Spectroscopic Devices For Diagnosing Laboratory Plasmas

be accepted in partial fulfillment of the
requirements for the degree of

MASTER OF SCIENCE

Victor Kantsyrev, Ph.D., Advisor

Alla Safronova, Ph.D., Committee Member

Ana De Bettencourt-Dias,Dr.Rer.Nat., Committee Member

Hans Moosmuller, Ph.D., Graduate School Representative

David W. Zeh, Ph. D., Dean, Graduate School

December, 2016

Abstract

The compact x-ray/EUV facility at the UNR Physics Department's Plasma Physics and Diagnostics Laboratory (PPDL) was improved to obtain high density and temperature plasmas with z-pinch plasma experiments and has been named Sparky II. The facility's energy storage capacity was doubled, electrical network remodeled, and its safety and control systems were reengineered. Vacuum spark experiments were performed and the improvements in the discharge capabilities will be shown. A gas-puff z-pinch system was developed for the Sparky II facility and results of characterization of the gas-jet will be discussed. Two new instruments were developed to measure parameters of plasma sources created with UNR's Sparky II Facility, Leopard laser, and Zebra generator as well as plasma sources created at other non-UNR z-pinch and laser plasma facilities. The first instrument is a horizontal focusing Johann type spectrometer designed to record spectra with high spectral resolution. The design of the spectrometer and spectra from plasmas formed in jets of noble gases created with both the UNR Leopard Laser and LLNL's Titan laser will be shown. The second instrument is a spectropolarimeter that was developed to record polarization sensitive plasma measurements. The device will record two sets of spectra with orthogonal sensitivities to polarization and 1D resolution in orthogonal directions. More future applications of these devices will be discussed.

Acknowledgements

I would like to think my advisor, Dr. Victor Kantsyrev, for all of the guidance, insight, and mentorship he provided throughout both my undergraduate and graduate studies and during the performance of the work presented in this thesis. I would also like to thank Dr. Alla Safronova for her advice and expertise during these times as well. This work would not have been possible if I had not had access to them and their abundance of knowledge and experience in plasma science and diagnostics. I also owe them thanks for the many scientific opportunities I have had the pleasure of participating in during my studies such as working with the Titan laser at LLNL's Jupiter Laser Facility. I extend my thanks to the other two members of my committee, Dr. Ana De Bettencourt-Dias and Dr. Hans Moosmüller for taking an interest in this research.

This thesis would not have been possible without the hard work of the other members of Dr. Kantsyrev's research group: Dr. Ishor Shrestha, Kim Schultz, Veronica Shlyaptseva, and Chris Butcher. They have all been not only helpful and supportive coworkers but also great friends. I would also like to thank Travis Coleman for the contributions he made to Johann spectrometer while working on his senior thesis. I cannot forget to also thank the members of Dr. Safronova's research group: Dr. Austin Stafford, Emil Petkov, Ryan Childers, and Max Schmidt-Petersen. They have been wonderful collaborators and friends.

The research presented here would have never been achievable without the all of the support received from UNR physics department's machine shop staff: Wade Cline and Carl Davidson. They have provided years of technical advice and machined countless parts for the experiments discussed here. My gratitude also goes out to the UNR physics department's chair, Paul Neill, as well as the administrative staff: Mercy Balderrama, Marvin Wakefield, Lindsay Reynolds, and Jordan Barker. I would like to thank them for their hard work in keeping the

department a welcoming place to get an education in physics. I want to thank Alexey Astonovitskiy, Vidya Nalajala, Oleksandr Chalyy, and Oleg Dmitriev for their support during experiments performed with UNR's Zebra Generator and Leopard Laser. I would also like to thank the staff of the Jupiter Laser Facility at LLNL.

I would like to thank my mom, Judy, my dad, Dan, and my brother, Ben, for their support and encouragement not only throughout this entire process but especially when things were at their toughest.

This work was supported by the DOE grants DE-NA0002954, DE-NA0003047, and DE-NA0001984, and in part by the DTRA grant HDTRA1-13-1-0033.

Table of Contents

List of Tables

List of Figures

Chapter 1: Introduction

This thesis covers the development of a high temperature and density laboratory plasma source as well as the development of plasma radiation diagnostics. There are several goals behind the performance of plasma science in University laboratories. One goal is to support the scientific community's efforts toward Inertial Confinement Fusion (ICF). The concept of ICF is to use radiation to compress and heat a small sample of deuterium and tritium until it reaches thermonuclear temperatures (Nuckolls 1982). Searching for cost effective, energy efficient sources of radiation in the extreme ultraviolet (10eV < EUV < 100eV), soft x-ray (100 eV < SXR < 5 keV), and hard x-ray (HXR > 5 keV) regions can provide information for designing future ICF experiments. Other goals of laboratory plasma science include: developing radiation sources for x-ray effects testing, x-ray backlighting, or x-ray lasers, creating and studying plasmas with parameters similar to those of astrophysical plasmas, calibrating radiation diagnostics for use with higher energy sources on larger plasma devices, and the teaching and training of physics students.

Two plasma radiation sources used in this research are laser-produced plasmas and z-pinches. Laser-produced plasmas can be formed when a short, intense pulse of laser light is focused on to a target which is typically a sample of solid material (see Figure 1.2) or jet of gas. The target material is heated or ionized by the radiation and a short-lived plasma is created. For example, a solid Cu target irradiated with a 0.4 J, 3 ns laser pulse can produce a two-temperature Cu plasma with electron temperatures of 20 eV and 90 eV (Weller *et al.* 2012). An 18 J, 350 fs laser pulse striking an Ar gas jet can produce a 750 eV Ar plasma (Kantysrev *et al.* 2016).

In a z-pinch plasma device, a load such as a wire array, foil liner, or gas-puff is situated between an anode and cathode (see Figure 1.1). A capacitive discharge is applied to the electrodes causing a current to flow through the load material. Depending on the material and discharge conditions, the material can form a plasma that is then pinched on

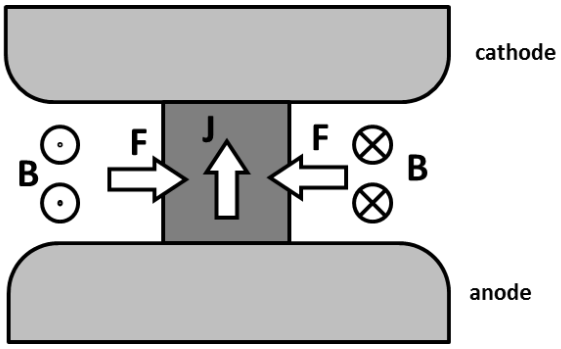

Figure 1.1: Illustration of a z-pinch plasma. J. current; B. magnetic field; F. Lorentz force. The sample material is shown in dark gray.

to its axis by the inward radial Lorentz force produced by the axial current and azimuthal magnetic field (Giuliani *et al.* 2012). An example of a z-pinch plasma is a Cu x-pinch wire array (see Figure 1.2d) imploded by a 1.7 MA, 100 ns current pulse to create a plasma with a temperature of 340 eV (Stafford *et al.* 2016). Laser-produced plasmas and z-pinch plasmas can all be used as powerful sources of x-ray and EUV radiation.

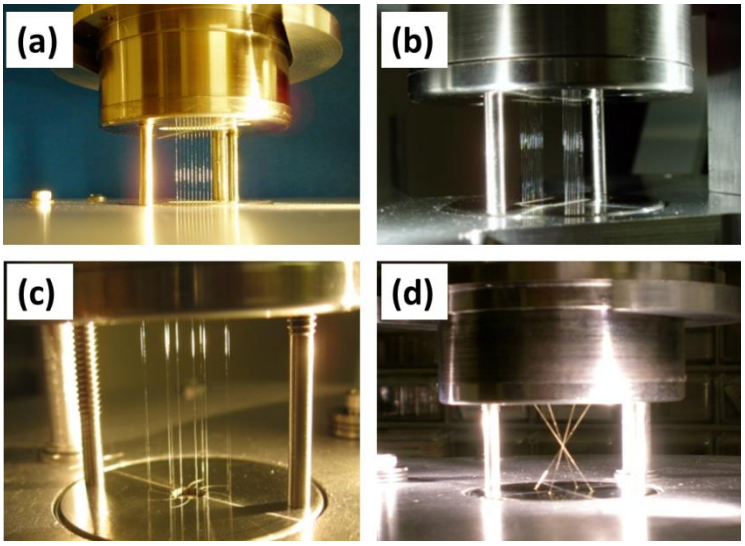

Figure 1.2: Photos of several different wire array z-pinch loads. a. Single planar wire array (SPWA); b. Double planar wire array (DPWA); c. Nested cylindrical wire array (NCWA); d. Symmetric X-pinch. The two outside supporting rods are removed before discharge of generator.

Two types of z-pinch plasmas discussed in detail in this thesis are those with vacuum-spark and gas-puff loads. A vacuum spark is typically triggered by an initial low temperature and density plasma jet that is injected in to the anode-cathode gap shown in figure 1.3. The electrons from this initial plasma are accelerated toward the anode and anode material is evaporated into the gap. The main discharge from a capacitive source is then triggered and the anode material is pinched on to the device's axis. Vacuum spark z-pinches are known to form small (1-500 μm), hot (200 eV to 10 keV), dense (10^{21}-10^{22} cm^{-3}), bright points of plasma during the rising current of the main discharge (Schulz *et al.* 1993). These bright points are effective sources of x-ray radiation. The renovation of a z-pinch generator as a vacuum spark radiation source and some initial results will be discussed in chapter two.

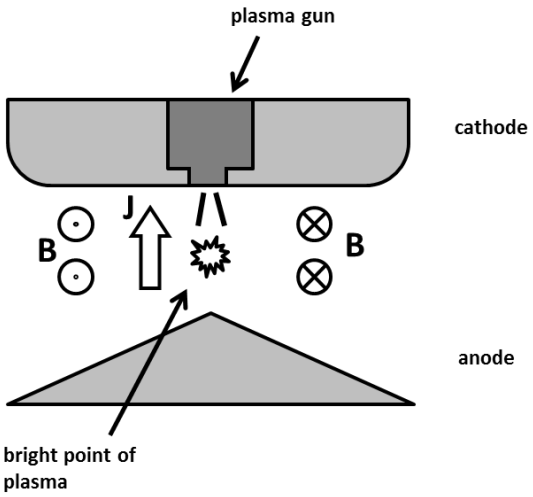

Figure 1.3: Illustration of a vacuum spark z-pinch. J. current; B. magnetic field.

A z-pinch with a gas-puff operates on the same principle as those created with wire-array loads or as a vacuum spark. The load in this case is a jet of gas injected into the anode-cathode gap by a valve at the cathode (see Figure 1.4). During the implosion, gas-puff z-pinches can form bright points similar to those in vacuum sparks (Schulz *et al.* 1993). The formation of these bright points is desirable if the goal is to create an effective source of bursts of x-ray radiation. However some research into gas-puff z-pinches is concerned with avoiding the formation of these points and increasing the duration and uniformity of the implosion to create longer, uniform pulses of radiation for ICF (Giuliani 2015). Chapter three will provide an overview of the development and characterization of a gas-puff z-pinch system for the pulsed power generator discussed in chapter two.

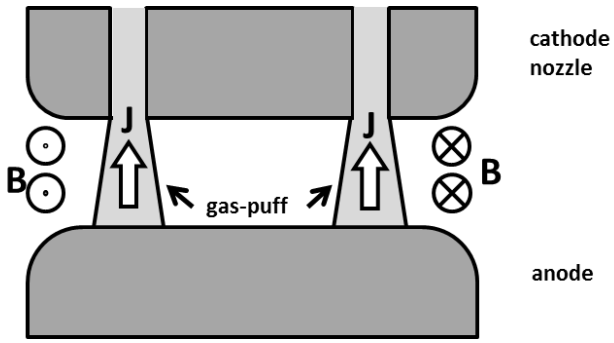

Figure 1.4: Illustration of a cross section of a cylindrical shell gas-puff z-pinch. J. current; B. magnetic field. The anode and cathode are shown in light gray and the sample material in dark gray.

Another example of a z-pinch plasma is the Mather type dense plasma focus. The plasma generating device consists of a coaxial anode and cathode filled with a gas in between. A bank of capacitors connected to the anode is discharged, the gas breaks down and a current flows radially between the anode and cathode forming a plasma sheath. The plasma travels along the axis of the device due the Lorentz force between the radial current and azimuthal magnet field. When it reaches the end of the anode, the plasma collapses down on to the device's axis in a pinch that can have an electron temperature of 0.1-1 keV.

Some of the most important tools for characterizing these radiation sources are x-ray spectrometers. This usually consists of using either a multilayer mirror or a crystal to spatially separate the different wavelengths of radiation coming from a source. This thesis will only discuss spectroscopy using crystals of known atomic spacing. When x-ray radiation is incident on a crystal's surface, radiation of a certain wavelength will be reflected from the surface depending on the grazing angle according to Bragg's law:

$$m\lambda = 2d\sin\theta \tag{1.1}$$

where m is the order of reflection, λ is the wavelength or radiation reflected, d is the spacing between atomic planes in the crystal, and θ is the grazing angle between the radiation beam and the crystal surface. X-ray spectrometers are often used with grazing angles near 90° so that the radiation reflected from the crystal will be close to its '2d' value of twice the crystal's atomic plane spacing.

The two essential components of spectrometers used to study x-ray sources are the crystal and the x-ray sensitive detector. There are many different geometrical configurations of these two elements that provide different advantages in terms of luminosity of the spectrometer, resolution of spectra on the detector, cost, and feasibility of construction and alignment. One configuration that is relevant to this thesis is the horizontal focusing scheme shown in Figure 1.5. In a horizontal focusing spectrometer, the crystal is curved into a concave cylindrical surface to focus radiation on to the detector (Johann *et al.* 1931). The x-ray source is placed somewhere in a plane perpendicular to the curved surface of the crystal and a boundary, called a Rowland circle, is imagined that has a radius half that of the radius of curvature of the crystal. If the source lies within this boundary then radiation reflected from the crystal can be resolved along the Rowland circle. By adjusting the source position, the optimal balance between spectral resolution and luminosity of the spectrometer can be obtained. One advantage of the horizontal focusing scheme is that the spectral resolution is not heavily dependent on the dimensions of the source. The details of a horizontal spectrometer developed to record x-ray spectra from K and L-shell ions of noble gas jet laser-plasmas will be discussed in chapter 4.

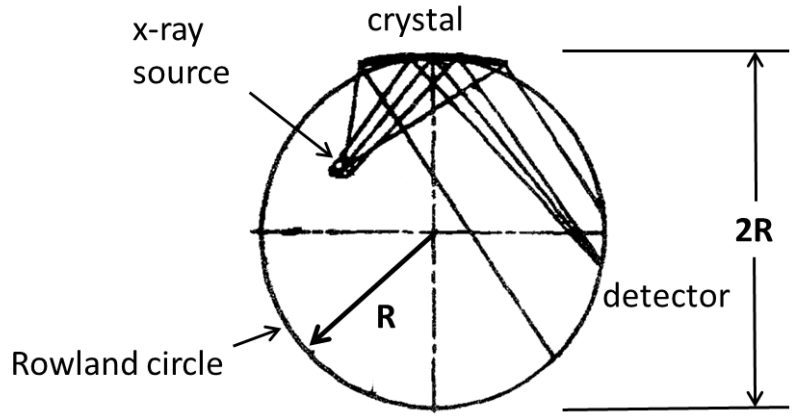

Figure 1.5: Illustration of a horizontal focusing concave crystal spectrometer. R. Rowland circle radius; 2R. Crystal curvature radius.

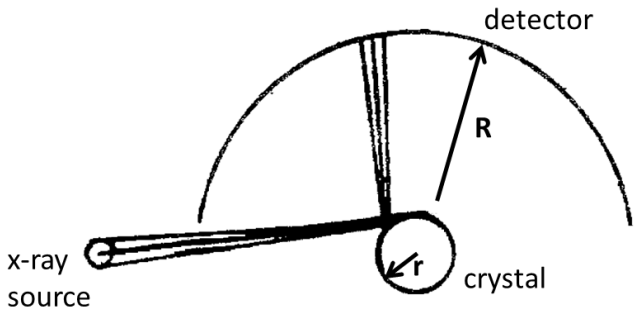

Figure 1.6: Illustration of a convex crystal spectrometer. r. Crystal radius; R. X-ray detector radius.

Another spectrometer configuration used in this research is the convex crystal spectrometer shown in Figure 1.6. As the name suggests this type of spectrometer uses a convex cylindrically bent crystal as opposed to the concave crystal used in a horizontal focusing spectrometer. One of the advantages of this type of spectrometer is the wide

spectral coverage that can theoretically record all wavelengths below that of the ‘2d’ value of the crystal (Aglitskiy *et al.* 1974).

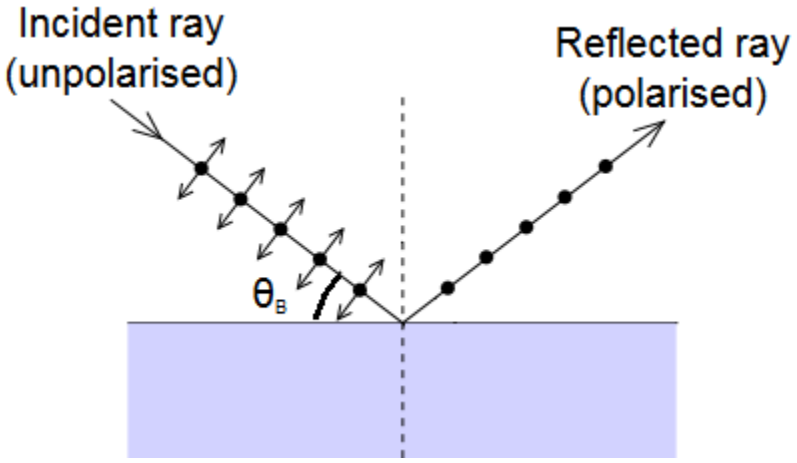

Figure 1.7: Illustration of a polarization by reflection for x-ray radiation incidence on a crystal.

The research in this thesis makes use of convex crystal spectrometers to peform polarization sensitive measurements. This is called spectropolarimetry and it takes advantage of polarization by reflection from two orthogonal crystals (Shlyaptseva *et al.* 2001). Polarization by reflection is most often discussed in terms of optical wavelengths reflected from a surface between materials of different indices of refraction (see Figure 1.7). If unpolarized light is incident on the surface, only the portion of the light polarized in the direction of the plane of the surface will be reflected if the angle of incidence is equivalent to Brewster’s angle. This angle depends on the indices of refraction of the two materials (Brewster 1815). Similarly, unpolarized X-ray radiation selectively reflected from a crystal only consists of the portion of the radiation polarized in the direction of the plane of the crystal if the angle of incidence is near 45°. This can be used to measure polarization of radiation from a plasma source by using two spectrometers with crystals placed at 90° from each other relative to the direction of the beam of radiation

(Shlyaptseva *et al.* 2001). If the spectrum at a certain wavelength is more intense on one spectrometer, then it can be inferred that the radiation is more polarized in the direction of that spectrometer's crystal plane. A spectropolarimeter based on this concept to make polarization sensitive measurements of L-shell ions from a Mo plasma will be discussed in chapter 5.

Chapter 2: Development of New Compact Pulsed Power Generator Sparky II

2.1 Motivation

The pulsed power section of the Sparky facility previously operated as a vacuum spark z-pinch generator as shown in Figure 2.1 (Kantsrev *et al.* 2004). The facility was capable of producing a 70 kA vacuum spark discharge at a voltage of 17 kV and a burst of x-ray radiation with 0.5-1.0 J of energy in the keV spectral band and up to 10-15 J energy in the sub-keV spectral band. This provided up to a 1.5% conversion efficiency from electrical to x-ray energy. One of the main goals of the renovation of the facility was to raise the maximum achievable current through the load. The purpose of this is to increase the total x-ray output energy of future experiments.

Another import goal during the renovations was to enhance the facility as a platform for studying laboratory scale plasmas. In order to support ICF efforts and expand plasma science, it is important to be able to characterize parameters of plasmas such as ion charge state, electron temperature, and electron density. This can be achieved through analyzing radiation captured using spectrometers. Temporal information about the plasma can be obtained using fast x-ray detecting diodes. Structural information about the plasma and its radiation can be obtained through the laser shadowgraphy and x-ray pinhole imagers, respectively. Providing an optimal setting to simultaneously make many of these measurements was equally as important as increasing the machine's output (see Figure 2.2).

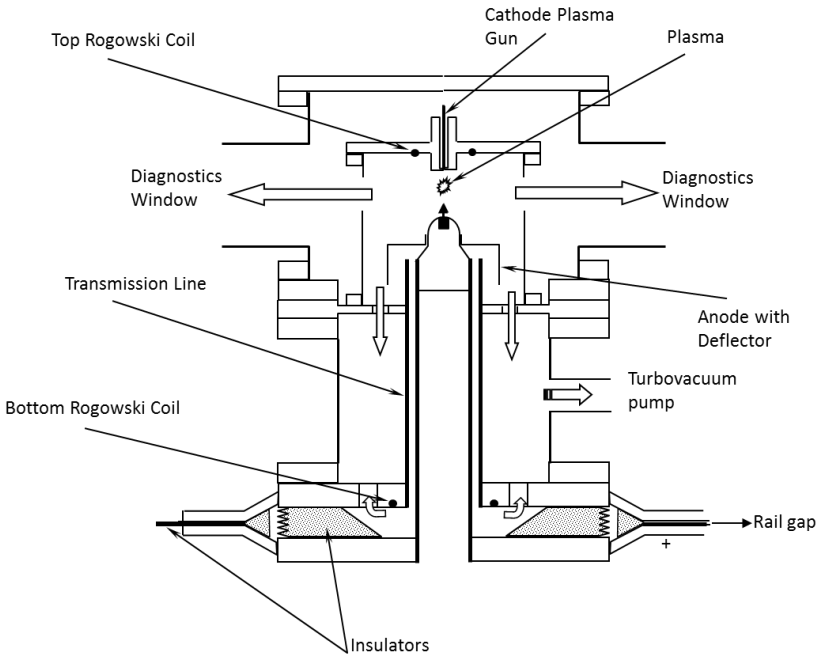

Figure 2.1: Illustration of Sparky facility vacuum spark experimental setup before renovation.

In order to accomplish the goals listed above, many systems must work simultaneously and in coordination with each other. Accuracy of timing is essential when stored energy is released in microseconds and radiation occurs in bursts of nanoseconds. Most of all the safety of personnel and equipment is a priority in a laboratory with high voltage equipment. Consequently, an important motivation of renovation of the facility was to improve control and automation of shot initiation and data collection. This includes both engineered and procedural controls.

The last motivating factor was to create an up-to-date laboratory environment for the education and training of UNR students. Ideally students in experimental high energy density physics should have the opportunity to run experiments creating a laboratory

plasma, collect data with various electrical and radiation diagnostics, analyze these data, and report on it at conferences and in their theses and dissertations. The work done here strives to establish the Sparky facility as a novel place for this to take place in the future.

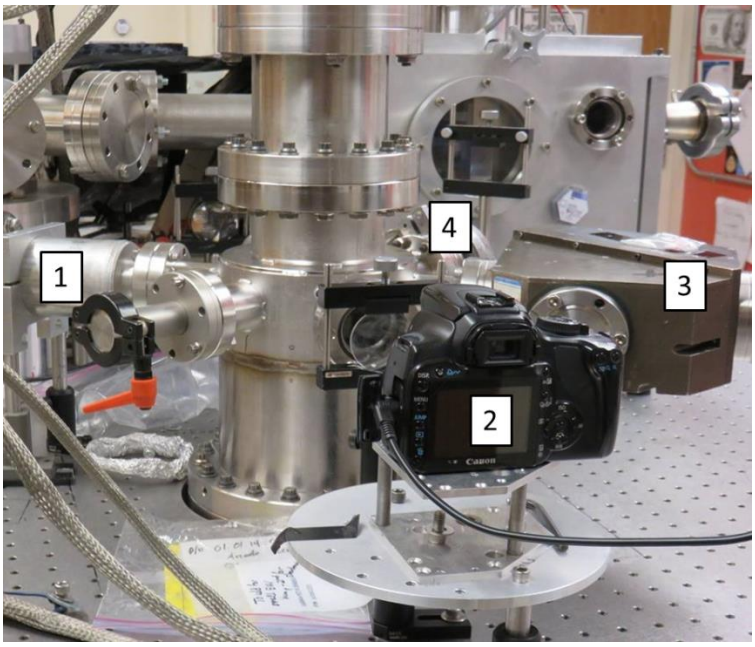

Figure 2.2: Photo of the Sparky facility diagnostic complex. 1. Three-channel head holding filtered PCD and Si-diodes; 2. Optical framing camera; 3. X-ray spectrometer with convex KAP crystal; 4. X-ray pinhole camera. Inside chamber: Current measuring Rogowski coil.

2.2 Improvements to Electrical Network

In an effort to increase the x-ray output energy, the machine was modified in two ways: the total energy storage capacity was increased and the electrical network's inductance was decreased. These two things were done to increase the total current while preventing the rise time of the pulse from becoming too long. Depending on the load used, the increased current can potentially be used to create hotter and denser plasmas that radiate more intensely.

The first task was to decrease the inductance. Figure 2.3 depicts the discharge chamber before renovation and Figure 2.4 shows the changes that were made to it (Cooper 2014a). In a coaxial cylindrical circuit, such as that formed by the device's

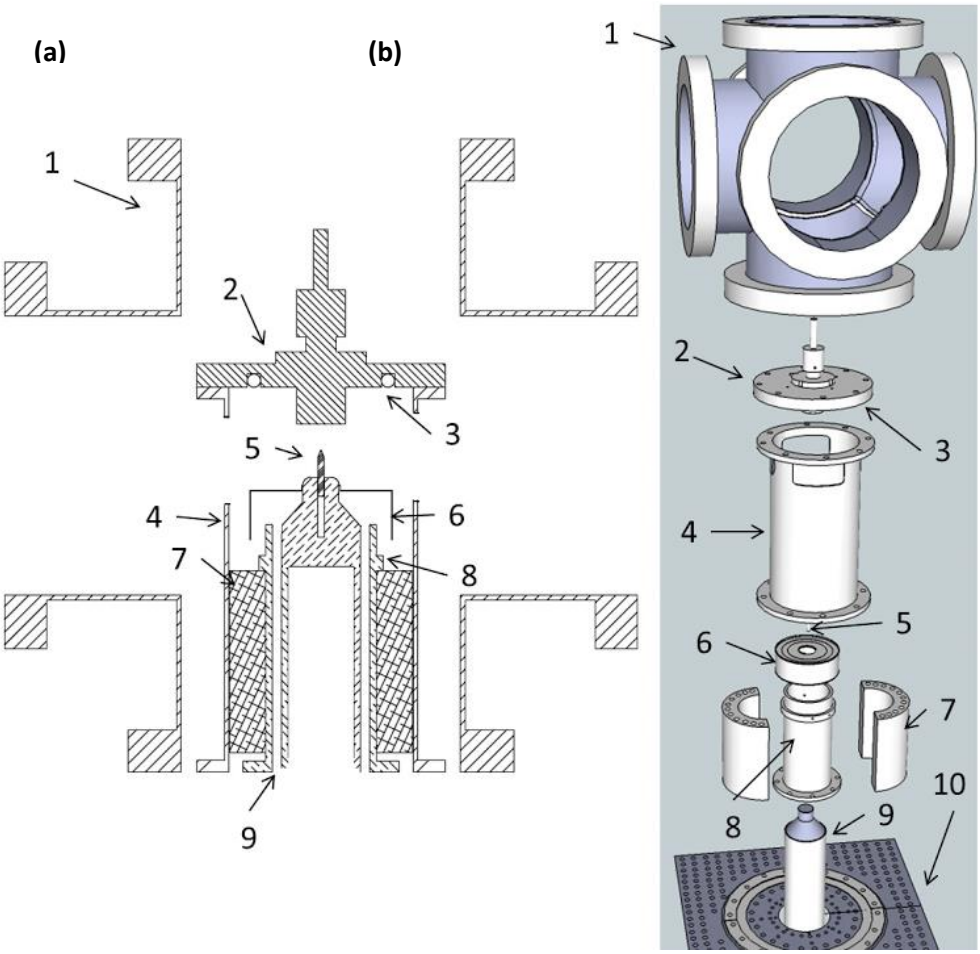

Figure 2.3: Schematics of the Sparky discharge chamber before renovation. This depicts the setup for vacuum spark experiments. a. Section view; b. Exploded view. 1. 6-way cross chamber; 2. Cathode with plasma gun; 3. Top Rogowski coil; 4. Outer return current shell; 5. Anode pin; 6. Arcing deflector; 7. Half cylinders; 8. Anode sheath; 9. Anode transmission line; 10. Grounded plate.

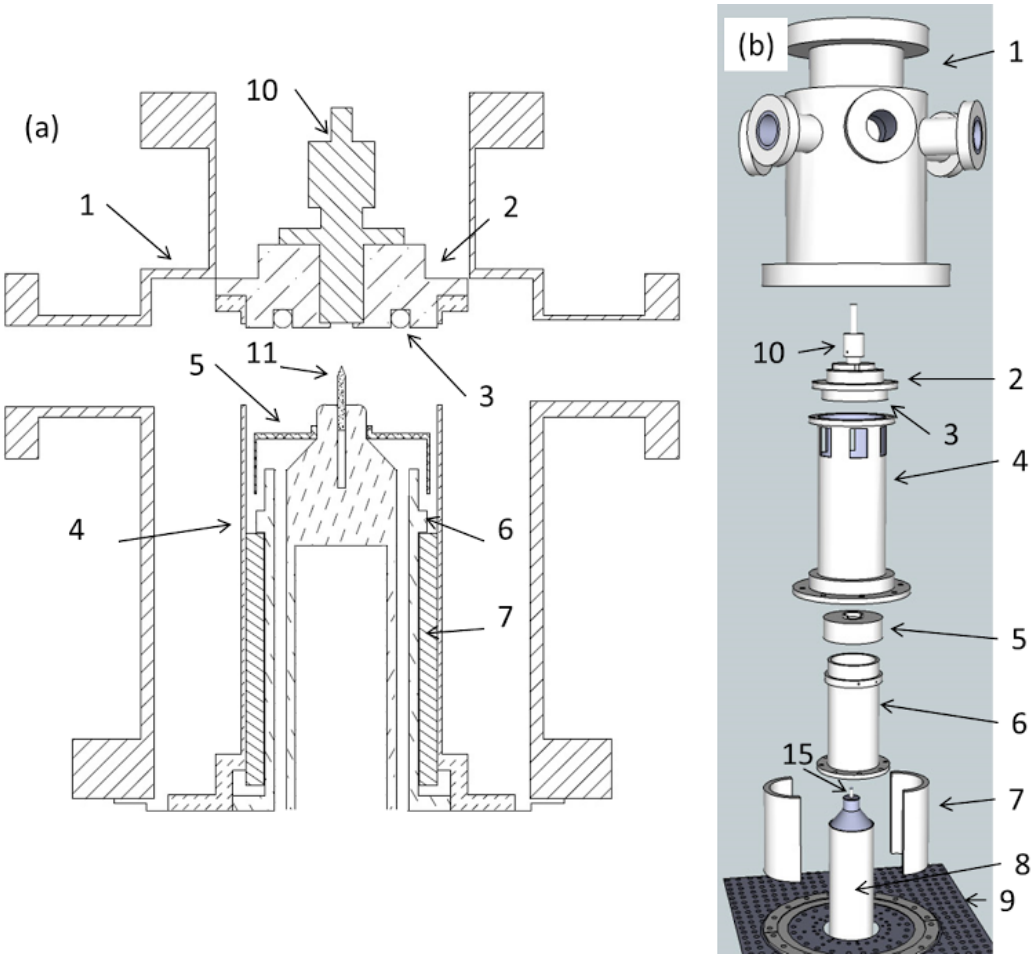

Figure 2.4: Schematics of the Sparky discharge chamber after renovation. This depicts the setup for vacuum spark experiments. a. Section view; b. Exploded view; 1. Eight-way Six-port chamber; 2. Cathode flange; 3. Top Rogowski coil; 4. Outer return current shell; 5. Arcing defletor; 6. Anode sheath; 7. Half cylinders; 8. Anode transmission line; 9. Grounded plate; 10. Plasma gun; 11. Anode pin.

anode and return current path, the self-inductance can be determined as follows:

$$L = \frac{\mu_0 l}{2\pi} \ln\left(\frac{b}{a}\right) \tag{2.1}$$

where L is the self-inductance, μ_0 is the permittivity of free space, l is the length of the coaxial circuit, b is the outer radius, and a is the inner radius (Serway *et al.* 2014). The inductance per unit length, L/l, depends on the ratio of the outer and inner radii. By

reducing the gap between these elements, the theoretical inductance of the electrical network was reduced from 20 nH down to 7.5 nH. The importance of low inductance can be illustrated by Eq. (2.2):

$$\boldsymbol{U = -L\frac{dI_{load}}{dt}} \tag{2.2}$$

where U is the anode-cathode gap voltage, and dI_{load}/dt is the steepness of the rise of current in the load. The current rise-time will be improved as the inductance is lowered. Other factors—for example, load type and geometry—affect the rise-time as well, but these geometrical changes were made to the circuit in an effort to provide a better base machine for different experiment types.

The other significant change made to the electrical network was the upgrading of its energy storage capacity. The main energy used during a discharge was stored in a bank of six parallel capacitors dubbed the Stinger Bank. Each unit was a Maxwell 31151 series 0.6 μF, 30 kV capacitor. With 23 kV applied by a General Atomics CCS power supply, up to 950 J could be stored in the Stinger Bank. Five additional 0.6 μF capacitors were added (see Figure 2.5) allowing up to 1750 J to be stored at the same voltage.

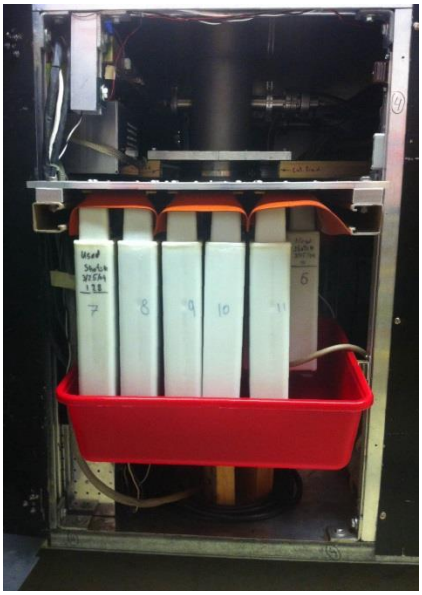

Figure 2.5: The Sparky II facility's Stinger Bank.

The facility's modified electrical network was modeled using the SCREAMER pulsed power circuit modeling code (Kiefer *et al.* 1999). It was shown that the theoretical maximum current, at full power supply voltage of 25 kV, could be increased from 130 kA to 200-230 kA (see Figure 2.6) by adding the five additional units to the Stinger bank. The near doubling in size of the Stinger Bank involved the development of a new brass hub to place the eleven capacitors in parallel and connect the Stinger bank to the Maxwell Laboratories 40200 Rail-Gap Switch that is triggered to initiate the main discharge. A new support chassis and interlocking cabinet door were also created to support the system and isolate it from personnel and other equipment.

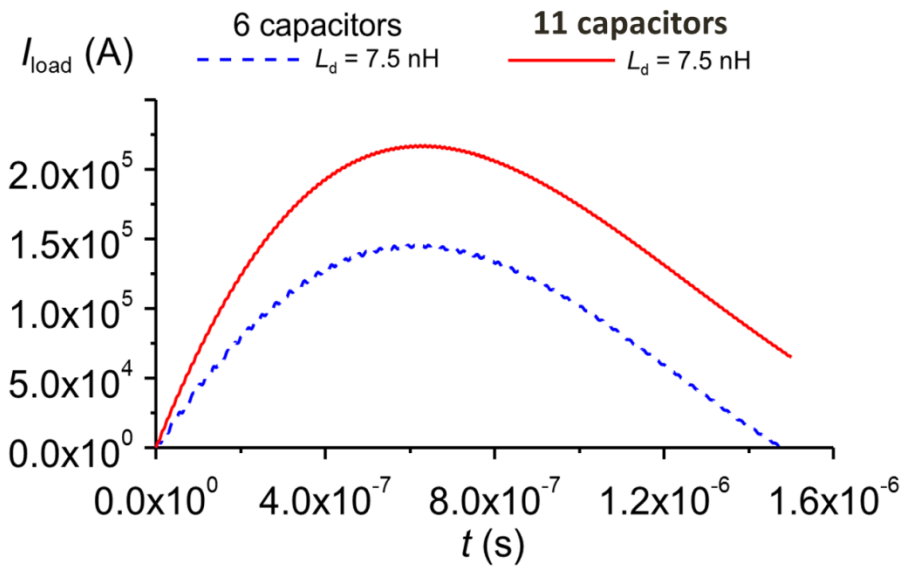

Figure 2.6: Modeling of the current, I_{load}, for "Sparky" versus time, t. The blue dotted line shows modeling of the current before expansion of the Stinger Bank and the red line shows modeling of the current after expansion. The modeling was done using the SCREAMER code with the help of Dr. Andrey Esaulov.

2.3 Improvements to Safety, Control, Data Acquisition, and Data Analysis

The data acquisition and control of the Sparky facility were originally developed to provide automation of the triggering of the seed plasma and main discharge as well as collection of electrical diagnostic data all via a computer terminal (see Figure 2.7a) running LabVIEW (Nalajala 2004). A LabVIEW front panel was created to trigger the BNC 555 delay generator from the computer. Once triggered, the delay generator would send four signals to the Sparky cabinet: a 3 second wide signal to enable high voltage on the Maxwell Power Supply, a 3 second wide signal to adjust the voltage level, a 1 μs wide signal with 3 second delay to trigger the Plasma Gun, and a 1 μs wide signal with a 3 second and 1-5 μs delay to trigger the Rail Gap Switch. Once triggered, the delay

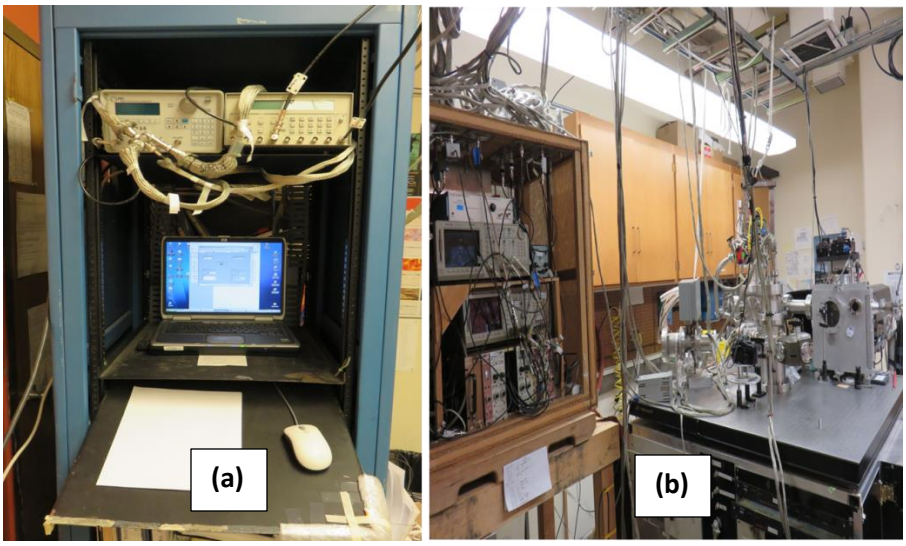

Figure 2.7: a. Photo of the computer with LabVIEW, Berkeley Nucleonics Corporation (BNC) 555 Delay Generator, and Stanford DG 535 Delay Generator used to control and trigger experiments; b. Photo of the Faraday cage containing a Tektronix TDS 640A four channel scope (top) and TLS 216 16 channel scope (bottom) used to record electronic diagnostics.

generator will also trigger the Tektronix TDS 640A and TLS 216 oscilloscopes which will record signals from electrical diagnostics during the shot (see Figure 2.7b). Another LabView front panel was programmed to collect the data from both oscilloscopes.

The existing power supply that charged the Stinger Bank was replaced with the newer General Atomics 25 kV power supply mentioned earlier and the control system was altered to accommodate it. A new module, dubbed the Reset Switch (see Figure 2.8),

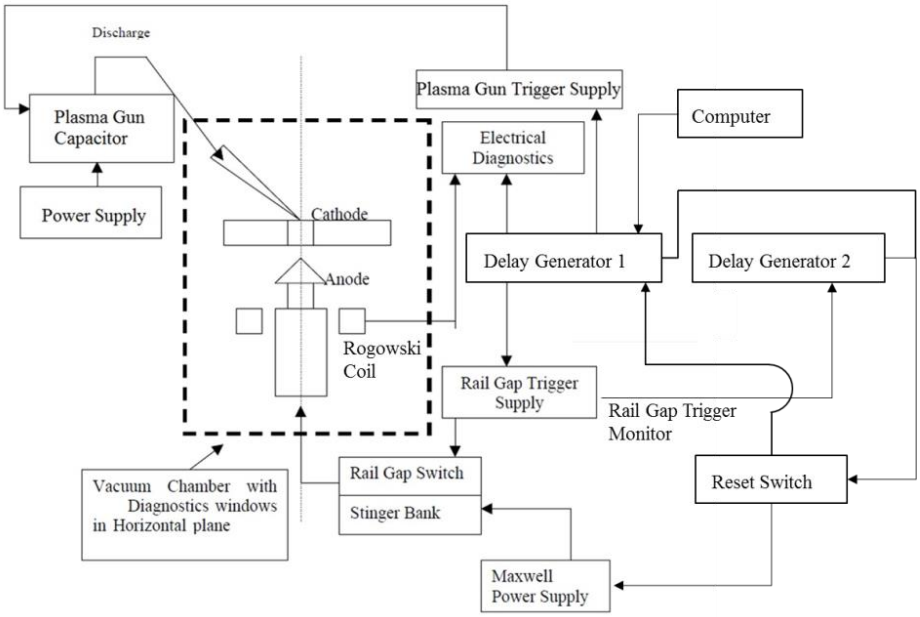

Figure 2.8: Block diagram of the controls and triggering method for a vacuum spark experiment on the Sparky facility.

was developed and installed in the Sparky cabinet. The Reset Switch was developed to do two things. Its primary function is to shut off the high voltage after a shot is initiated to prevent the power supply from recharging the Stinger Bank. Its secondary function is to shut down the power supply in the event that the Rail Gap Switch self-triggers so that further self-triggering is inhibited.

To accommodate this new system, a Stanford DG 535 unit (Delay Generator 2 in Figure 2.8) was added in addition to the BNC 555 (Delay Generator 1). Delay Generator 2 is triggered by Delay Generator 1 when a shot is initiated or by the Rail Gap Trigger Monitor in the event that the Rail Gap Switch self-triggers. The Rail Gap Trigger Monitor is a small solenoid inside the Rail Gap Trigger Supply unit that monitors for a changing magnetic flux induced from the discharging of the Stinger Bank when the Rail Gap Switch is triggered. Once the reset switch receives either signal it opens a small relay

that is connected to the high voltage interlock in the General Atomics power supply. This safely turns off the high voltage supplied to the Stinger Bank to prevent it from recharging and preventing possible further self-trigger events in the Rail Gap Switch. A manual toggle on the Reset Switch unit allows the high voltage to be re-enabled. The safety system was implemented so that a facility user can still trigger the machine and collect electrical diagnostic data all from the computer terminal.

The data analysis of current and x-ray burst signals was also streamlined during the renovation process. An important diagnostic in assessing the performance of the machine is the Rogowski Coil (see Figures 2.1, 2.3, 2.4, and 2.8) which is used to provide

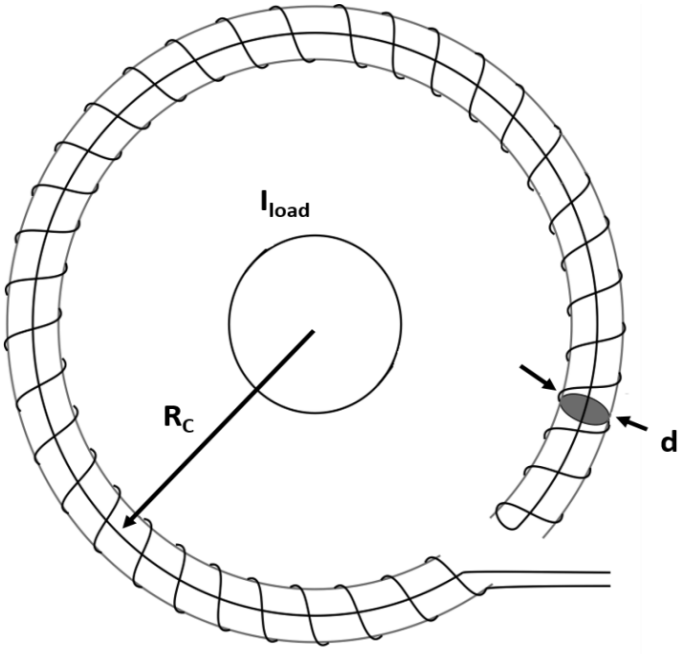

Figure 2.9: Illustration of a Rogowski coil used to the measure the current through a load. I_{load}. Current through the load ; R_C. Radius of the Rogowski coil ; d. diameter of one loop of the coil (Alfredo 2011).

time resolved data about the current. The Rogowski coil consists of a solenoid bent into a loop enclosing a section of the inner current path in the discharge chamber (see Figure

2.9). The coil's signal is governed by:

$$U_{coil} = -\mu_0 nA \frac{dI_{load}}{dt} \quad \textbf{(2.3)}$$

where U_{coil} is the voltage induced in the Rogowski Coil, n is the number of turns per unit length in the coil, and A is the area of one loop in the coil (L.A. Kojovic 2010). The load current can be obtained by integrating the Rogowski Coil signal. For the circular coil used in the Sparky facility, this becomes:

$$I_{load} = -\frac{8R_c}{\mu_0 N d^2} \int U_{coil} dt \quad \textbf{(2.4)}$$

where R_c is the radius of the coil, N is the total number of turns, and d is the diameter of a loop.

A spreadsheet was developed to process the Rogowski Coil signal and provide time resolved current information for a given shot as in Figure 2.11. It takes into account the above geometrical considerations, signal attenuation, and Stinger Bank voltage. The spreadsheet also takes in and displays signals from x-ray detecting diodes to consolidate information about each shot. The spreadsheet can be accessed on Sparky's computer terminal to allow for the assessment of shot characteristics in real time while performing experiments.

2.4 Results of Testing of Sparky II Facility

After renovation the Sparky II facility's pulsed power capabilities were tested with several vacuum spark experiments (see Table 2.1). The anode pin used was made

Sting. Bank [V]	Charge in Bank [C]	Peak current [A]	Rise Time [μs] (10% to 90%)	Rise Time [μs] (0% to 100%)
10000	0.066	51300	1.80	2.88
10000	0.066	51900	1.88	2.84
12500	0.0825	84000	0.96	1.56
12500	0.0825	93300	0.96	1.52
12500	0.0825	72700	0.98	1.48
12500	0.0825	88200	0.93	1.44
15000	0.099	109000	0.94	1.42
12500	0.0825	85300	1.03	1.51
15000	0.099	97600	0.96	1.69
15000	0.099	88800	1.04	1.95
17000	0.1122	111000	1.10	1.63

Table 2.1: Stinger bank voltage, charge, peak current, and rise time for several vacuum spark experiments performed on the Sparky facility.

from Cu (see Figure 2.4), and the gap between the anode and the cathode plasma gun was 9 mm. Several tests of only the plasma gun were performed (see Figure 2.10a) and the maximum current produced by the plasma gun alone was measured to be about 2 kA. Then high voltage tests were performed with Stinger Bank voltage ranging from 10 to 17 kV. Average rise-times of 1.5 μs were achieved with this vacuum spark configuration (see Table 2.1). The highest current achieved to date was 111 kA with a Stinger Bank voltage of 17 kV (see Figure 2.11). This was roughly doubled the current achieved at 17 kV with the system setup in the vacuum spark regime before renovation as shown in

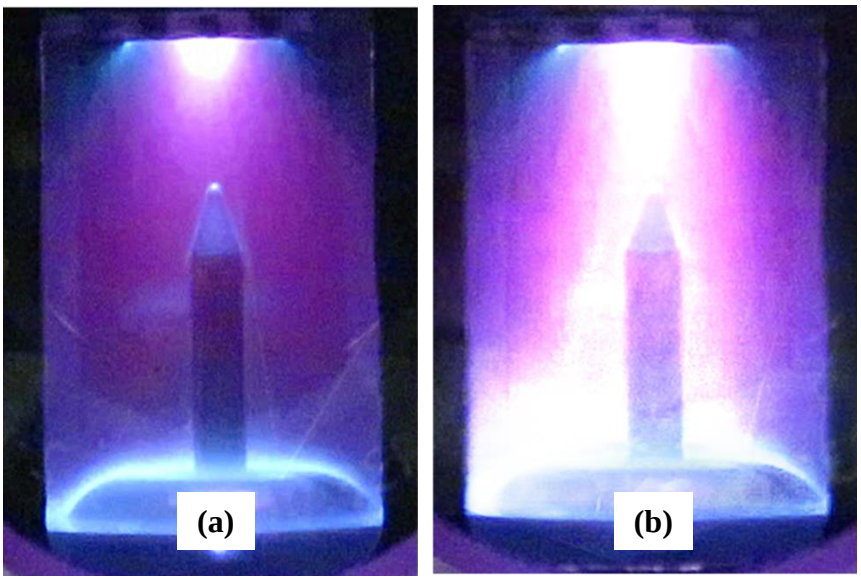

Figure 2.10: Optical image of the anode-cathode gap during a vacuum discharge experiment on the Sparky facility. a. A discharge with only the plasma gun ; b. A 10 kV discharge using the Stinger bank in addition to the plasma gun.

Figure 2.1. The optimal gap voltage for producing highly radiating bright points of plasma is 12.5-17 kV as shown in Zver'kov *et al.* 1986. The results of the vacuum spark tests are plotted in figure 2.12. The line of best fit suggests that currents of up to 150-170 kA are achievable with Stinger Bank voltages of 20-23 kV in the vacuum spark configuration.

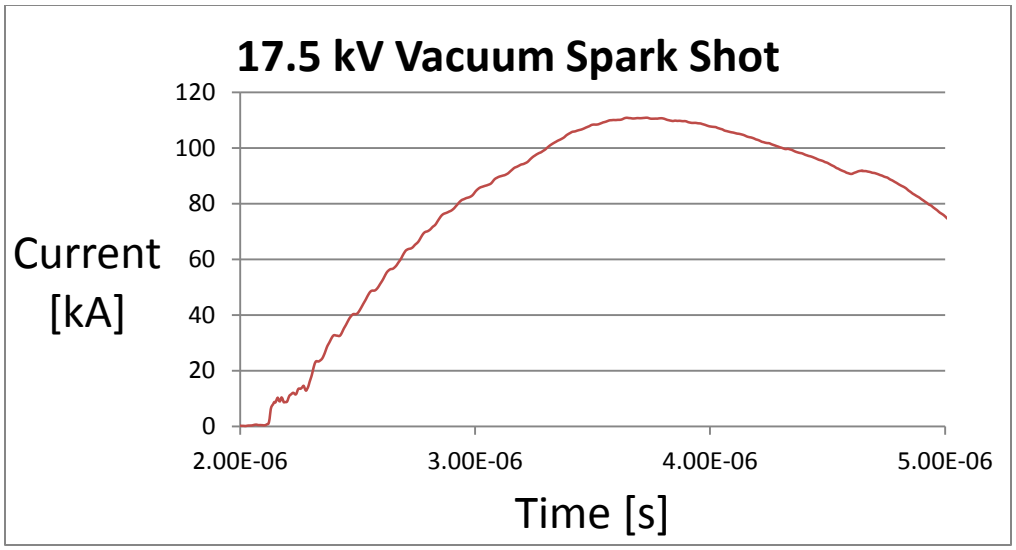

Figure 2.11: Current from a Sparky II vacuum spark experiment. The Stinger bank voltage was 17.5 kV.

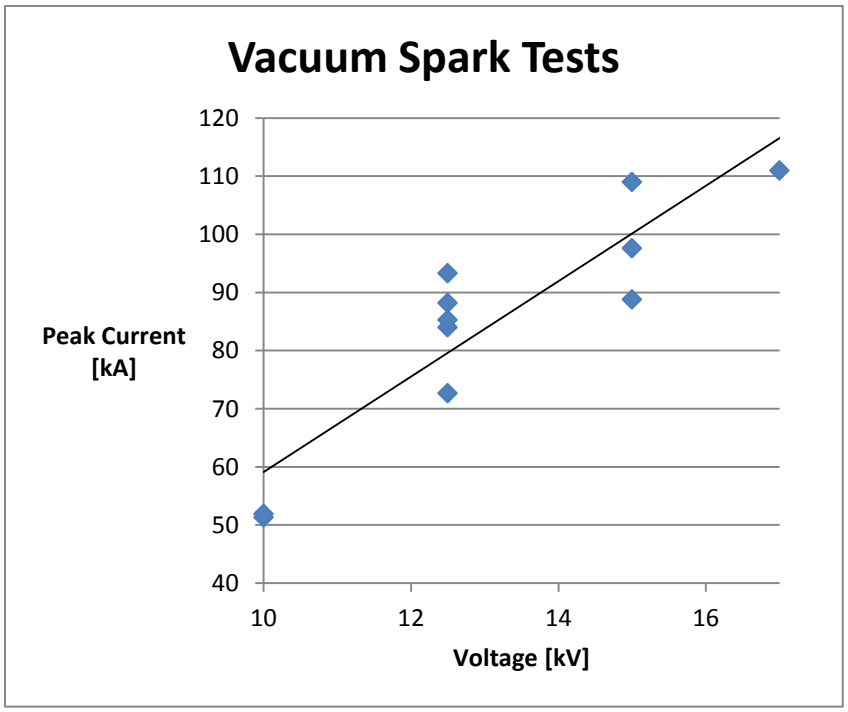

Figure 2.12: Peak current vs. voltage and trend line for several vacuum spark experiments performed on the Sparky facility.

The changes to the electrical network have markedly improved the performance of the facility as a vacuum spark z-pinch generator. Experiments performed in 2004 with a 17 kV Stinger Bank voltage were able to achieve currents of up to 70 kA but results of 40-60 kA were typical (Nalajala 2004). Tests performed after renovation showed that currents of up to 111 kA at the same stinger bank voltage were achieved. The changes to the control and data acquisition have also been successful. Shot initiation, electrical diagnostics data collection, and current analysis are all performed via the computer terminal. The Reset Switch disables the high voltage power to the Stinger Bank after a shot is initiated or a signal is received that the Rail Gap Switch has triggered. With these changes the Sparky facility remains an up-to-date platform for performing not only vacuum spark z-pinch experiments but investigating other radiation sources such as gas-puff z-pinches.

Chapter 3: Development of Gas-puff System for Sparky II

3.1 Motivation

In the search for energy efficient and cost effective sources of x-ray radiation, the gas-puff z-pinch has been seen as a source with many inherent advantages. Unlike wire array loads which must be replaced between every shot, a gas-puff load does not require opening the vacuum chamber and releasing the vacuum between experiments. This allows for a high repetition rate. The gas-puff load also has an advantage in initial density distribution. A gas-puff load can be made that is symmetric to the z-axis with the use of an axially symmetric nozzle. However, a load composed of individual solid wires will always vary along the azimuthal direction (Giuliani *et al.* 2015). The motivation for the creation of the Sparky gas-puff system is to characterize Ar and Kr gas-puff z-pinches as source of K-shell and L-shell radiation from a lower current machine (<200 kA). This data could be useful for planning gas-puff experiments on higher current machines (~15 MA).

3.2 Design of Gas-puff System

The gas-puff system was designed to utilize as much of the existing infrastructure of the z-pinch generator as a possible (see Figure 3.1). The power supply and circuitry for the plasma gun in the vacuum spark system are used to power the gas pre-ionization unit in the gas-puff system. The existing Maxwell Power Supply, Reset Switch, Stinger Bank, and Rail Gap Switch are still used to provide the anode-cathode gap voltage that induces the main current discharge. The existing system is mainly modified by replacing the cathode and anode. The cathode flange used in the vacuum spark setup (item 2 in Figure 2.4) rests on top of the outer current path and holds the plasma gun and top Rogowski

coil. This is removed and replaced with an alternative cathode flange (see Figure 3.2) that holds the main components of the gas-puff system and the top Rogowski coil. The existing anode pin (item 11 in Figure 2.4) is replaced with an anode that consists of a cone and a hollow disk. The same control and data acquisition system is used with only a few modifications. The DG 535 (Delay Generator 1) which previously triggered the plasma gun and Rail Gap Switch in the vacuum spark setup now triggers the Pre-ionization Unit, the Fast Valve Trigger Unit, and the Rail Gap Switch. All other existing systems for high voltage safety and data collection remain the same.

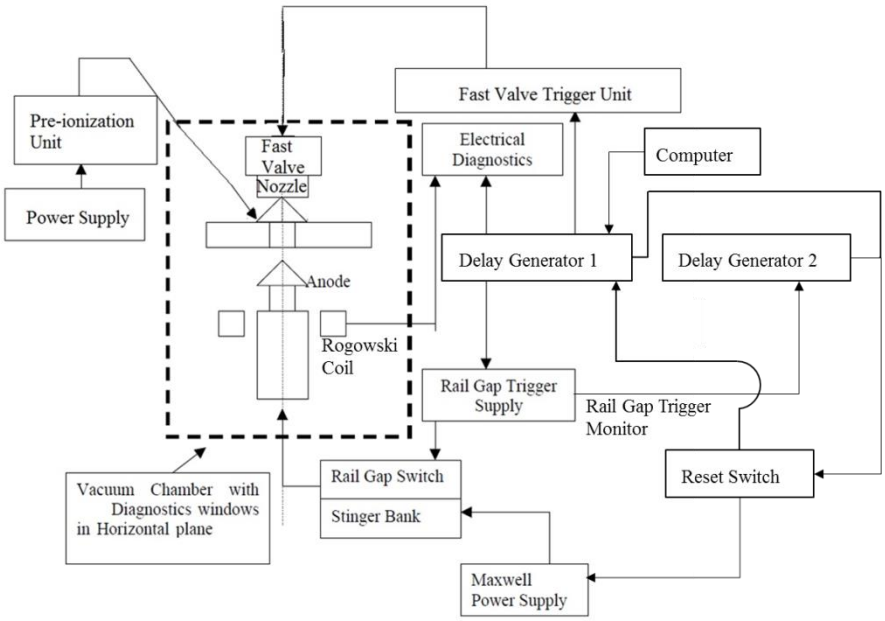

Figure 3.1: Block diagram of the controls and triggering method for a gas-puff z-pinch experiment on the Sparky II facility.

The main new components of the gas puff-system are the valve, nozzle, Pre-ionization Unit, cathode, and anode (see Figure 3.3). The valve used is a Parker Series 9 pulsed valve. It can be used with backing pressures of 400-600 PSI and can have an

opening time as low 160 μs. The valve is triggered with a 12 V pulse delivered by the Fast Valve Trigger Unit when it receives a signal from the DG 535 (Delay Generator 1). The valve then releases a small amount of gas which passes through the nozzle. The gas-puff system is designed to hold interchangeable nozzles that fit up into a Swagelok fitting in the fast valve and then rest just above the Pre-ionization Unit at the bottom surface of the cathode flange. The two currently available nozzles have conical inlets, narrow throats (0.5 mm and 1 mm diameters), and conical outlets (see Figure 3.4). The purpose of the valve and nozzle is to release a dense, pressurized puff of gas into the chamber.

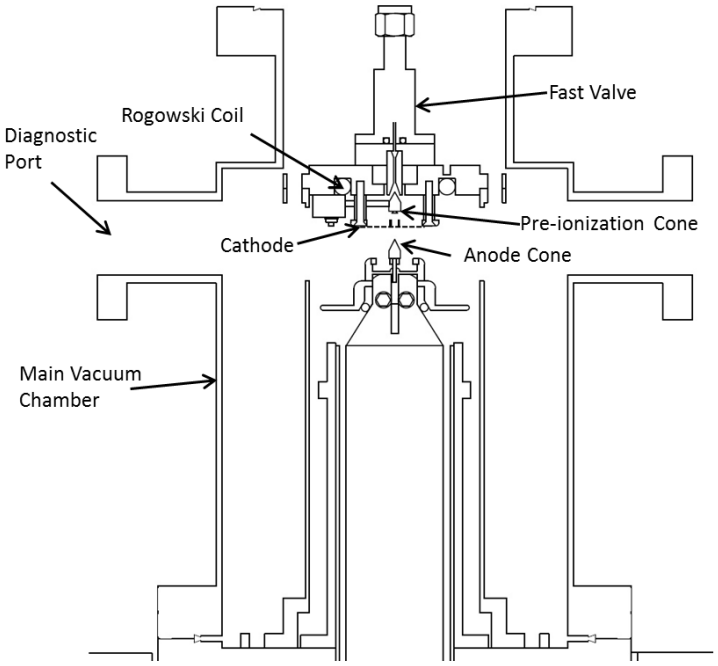

Figure 3.2: Schematic of the Sparky discharge chamber after renovation. This depicts the setup for gas-puff z-pinch experiments.

After exiting the nozzle, the gas reaches the Pre-Ionization Unit. This part of the system has two purposes. It forms the gas into a hollow cylinder shape before entering the anode-cathode gap and pre-ionizes it. An insulated rod holds a small tungsten-copper

alloy cone called the Pre-Ionization Cone (see Figure 3.3). The cone's shape matches the

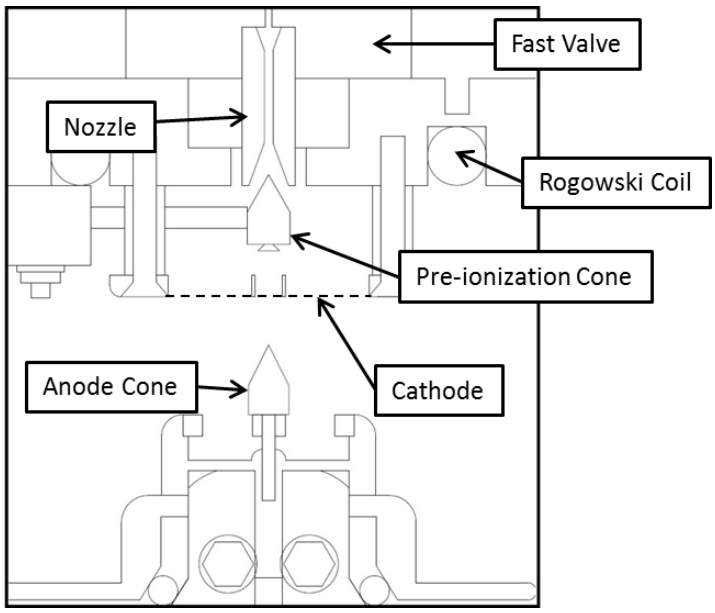

Figure 3.3: Schematic of the gas-puff z-pinch module designed for use inside the Sparky discharge chamber. The design is based on the results of the work done in Kantsyrev *et al.* 1994.

contour of the nozzle outlet. As the gas exits the nozzle and passes the Pre-Ionization cone, this contour matching is mean to create a column of gas with less density on axis. Gas-puff experiments can be done with neutral gas jets or pre-ionization of the gas can be performed to create an initial current pathway for the main discharge. To do this, a voltage between 200 and 500 V is placed on the Pre-Ionization Cone in either a steady state or as a pulsed configuration. The voltage used is chosen based off the breakdown properties of the gas. As the gas passes between the charged cone and the grounded nozzle, partial ionization of the gas can occur if a high enough voltage is applied. The minimum threshold voltage for breakdown has a biphasic relationship to the product of the gas pressure and gap distance according to Paschen's law as shown in Figure 3.5 (M.A. Lieberman *et al.* 2005). For example, if the average density of Ar gas between the

nozzle and pre-ionization cone is 2×10^{18} cm^{-3} and standard temperature is assumed, then the pressure will be about 60 torr. The distance between the nozzle and pre-ionization cone is about 0.15 cm giving a pd value of about 10 torr cm. According to Figure 3.5, this will require a minimum of about 400 V for the breakdown of Ar gas.

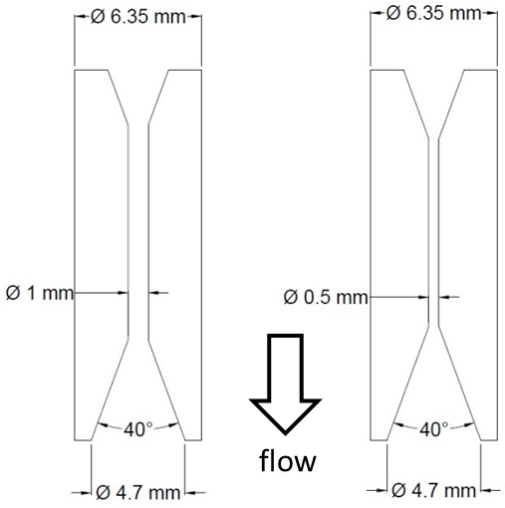

Figure 3.4: Schematic of the conical nozzles designed for use in the Sparky gas-puff z-pinch module.

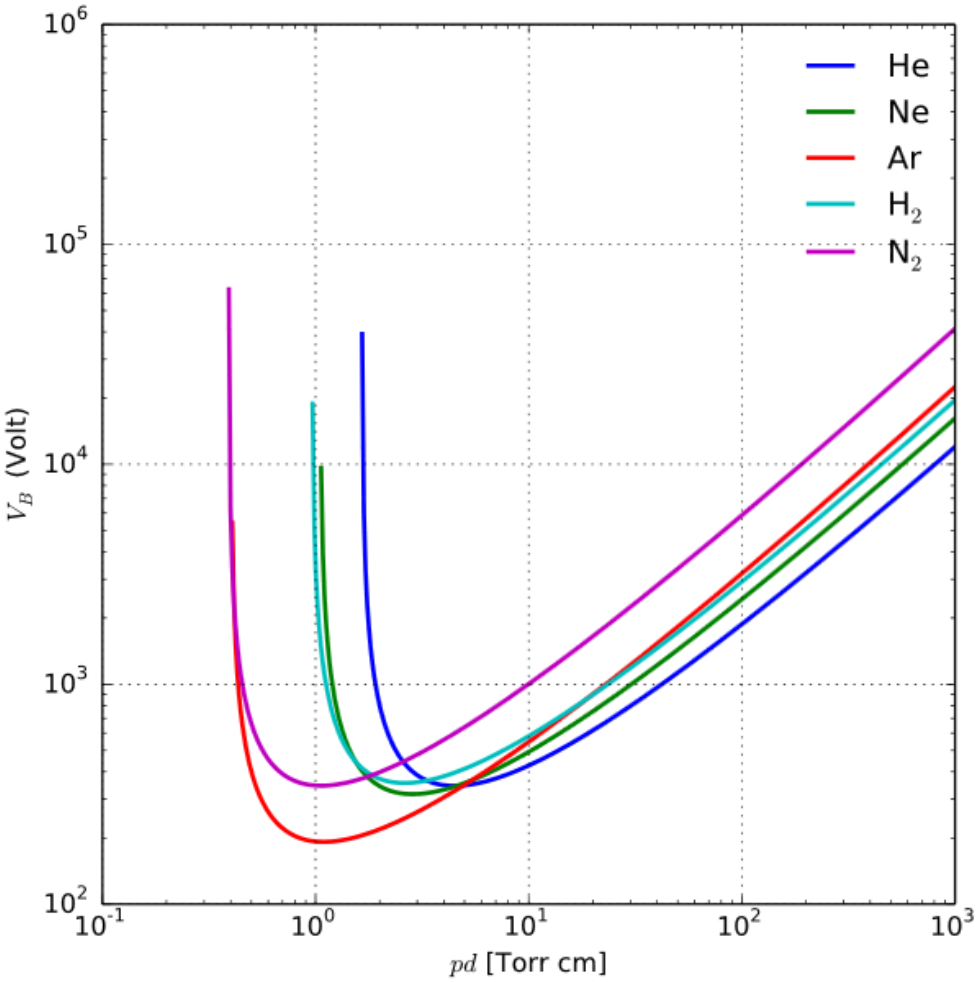

Figure 3.5: Paschen curves for several gases. V_B is the breakdown voltage and pd is the product of pressure and gap size (Krishnavedala 2014).

After passing the Pre-Ionization unit, the gas passes through the cathode. The cathode is formed by a disk with three holes that allow the gas to pass through (see Figure 3.6). The cathode is shaped this way to maintain the density profile of the gas as it passes through. The anode consists of a central cone and hollow tub below (see Figure 3.3). The central cone is used to create a more stable discharge. The electric field will be strongest near the tip of the cone since the gradient of the potential will be largest at this spot. A tungsten-copper cone is depicted in Figure 3.3 but the anode cone can be easily

replaced to try cones of other materials. The anode contains a hollowed out space below the cone to allow the gas to pass the anode with minimal disturbance. The physical components of the gas puff system were designed this way to provide several benefits to the experimenter: the nozzle is interchangeable, experiments can be formed with or without pre-ionization, and the anode material is interchangeable.

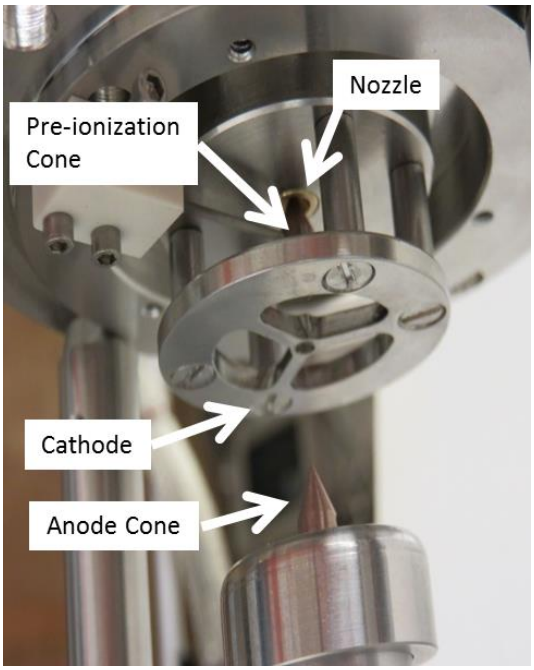

Figure 3.6: Photo of the gas-puff Z-pinch module designed for use in the Sparky discharge chamber.

3.3 Characterization of Gas-puff Z-pinch System

An important consideration with the gas-puff z-pinches is the density profile of the gas jet before implosion. With wire array loads, the density profile is known from the density of the wire material and the geometry of the load. With gas-puffs the initial density profile must be measured. For the Sparky gas-puff system this was done with a Mach-Zender interferometer setup at UNR's Radiation Physics Laboratory (RPL). The

532 nm wavelength beam from a pulsed Nd:YAG laser is split into a reference arm as well as scene arm that passes through the gas jet. The scene arm and reference arm recombine and focus on to a CCD detector giving a 2D inteferogram of the gas jet. The interferogram provides the phase shift of the light passing through the gas jet. This can be used to determine the density profile of the gas jet according to the Gladstone-Dale relationship (Moschella *et al.* 2011):

$$\boldsymbol{\Delta\varphi = \left(\frac{2\pi}{\lambda}\right)\int(n-1)dl = \kappa M\left(\frac{2\pi}{\lambda}\right)\int N dl} \quad \textbf{(3.1)}$$

where Δφ is the phase of the laser light, λ is the wavelength of the laser light, n is the linear mass density of the gas, dl is an infinitesimal line element along the laser path, κ is the Gladstone-Dale relationship, M is the atomic mass of the gas molecules, and N is the number density of gas molecules. From this equation, the line integrated density of the gas can be obtained from the phase shift and a 2D density plot like that shown in Figure 3.7 can be created.

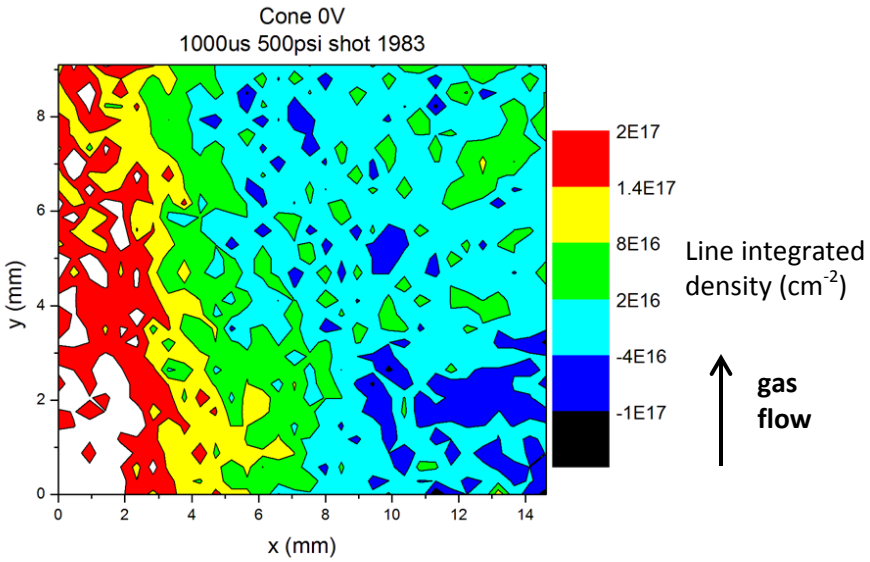

Figure 3.7: Line integrated density map of the Ar gas jet in the anode-cathode gap of the Sparky gas-puff system with a 500 PSI backing pressure and using the nozzle with the 0.5 mm throat diameter.

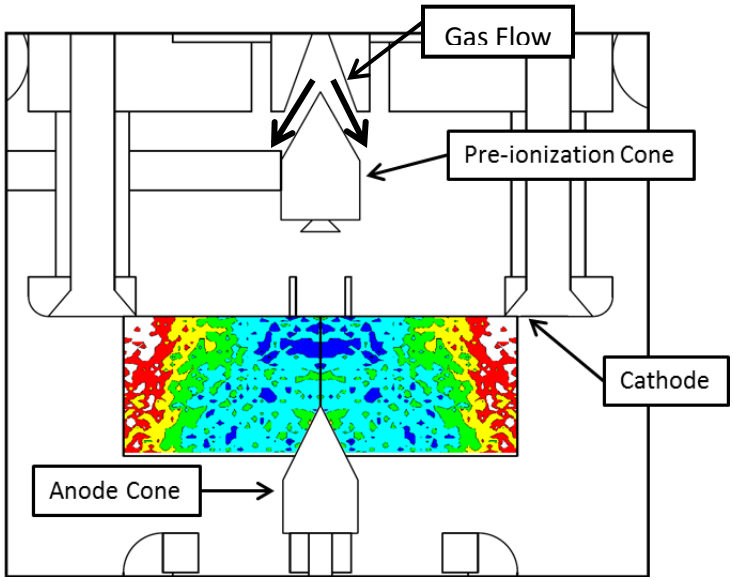

Figure 3.8: The line integrated density map from figure 3.7 inserted into the schematic of the Sparky gas-puff system anode-cathode gap. The density map is mirrored on to the other side of the anode-cathode gap to illustrate the approximately hollow shell structure of the gas jet which is use for typical gas-puff z-pinch schemes.

Several interferometry measurements of the Sparky gas-puff system's gas jet were taken with different backing pressures, gas delay times, with or without different pre-ionization voltages, with the two different nozzles, and above and below the cathode. Figure 3.7 is an interferogram of an Ar gas jet emitted with a 500 PSI backing pressure, 1000 μs gas delay time, without pre-ionization voltage, with the 0.5 mm throat nozzle, and below the cathode. With the inteferogram inserted to scale in a schematic of the anode-cathode gap, it is clear that the desired hollow shell density profile is achieved.

Chapter 4: Development of the Horizontal Focusing Johann Spectrometer

4.1 Motivation

Convex crystal spectrometers have the advantage of having wide spectral coverage but this comes at the expense of resolution. The resolution of these spectrometers can be improved by increasing the distance from the source to the crystal but that then comes at the expense of transmission (Aglitsky *et al.* 1974). Concave crystal spectrometers provide an alternative that doesn't suffer from these disadvantages. The focusing nature of a concave crystal allows for greater transmission of radiation on to the detector. The radiation focusing also allows high resolution to be achieved without needing to place the crystal far from the source. A convex crystal spectrometer is often sufficient for large x-ray sources like the UNR Zebra generator which has an x-ray output of 30 kJ. For a source like Sparky, which typically has x-ray outputs less than 15 J, the transmission of a typical convex crystal spectrometer would not be sufficient. Several tens of shots would need to be performed in order to collect enough radiation to activate the detector and provide useful spectra. However, in vacuum spark z-pinch experiments like those performed on Sparky, the main source of x-ray radiation comes from the formation of plasma points that vary in location between the anode and cathode. This spread in x-ray source location from shot to shot would reduce the resolution of the spectra obtained after several shots. One of the reasons for the development of the Johann spectrometer was to obtain spectra from single shots on the Sparky facility. Another motivating factor behind its development was to record K-shell Ar, L-shell Kr, and M-shell Xe spectra from laser-produced plasmas of noble gases.

4.2 Design of New Version of the Johann Spectrometer

The Johann spectrometer was designed with adjustability in mind (see Figure 4.1). The spectrometer was made small enough to be used in a diagnostic beamline or to be mounted to the floor of larger experimental chambers as depicted in figures 4.2(b) and 4.2(c). In the latter case, the height of the spectrometer can be adjusted over a range of about 20 cm as shown in the three different positions depicted in figure 4.1. The spectrometer also has two perpendicular translational directions with fine adjustment to aid in alignment. The detector, a filtered cassette containing x-ray film, can be switched between three different positions depending on the desired spectral bandwidth. One disadvantage of focusing spectrometers is their narrow bandwidth. The above features were implemented to circumvent this problem by allowing the spectrometer to be quickly adjusted between shots to observe different spectral ranges without altering the position of the source. The spectrometer was tested with a 15 J laser-plasma source and the obtained spectrum will be discussed in the next section. These first tests revealed three areas where improvements could be made.

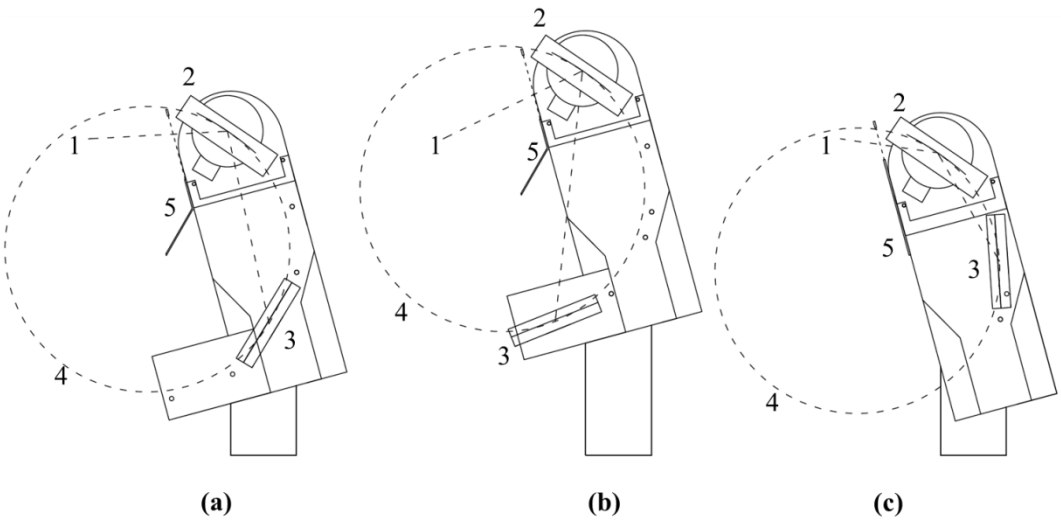

Figure 4.1: Schematic of the Johann spectrometer adjusted to record radiation in the regions: a. 3.9 Å – 4.58 Å (K-shell Ar); b. 5.26 Å – 5.73 Å (L-shell Kr); and c. 2.7 – 3.15 Å (M-shell Xe). 1. Radiation source; 2. Selectively reflecting crystal; 3. Detector; 4. Rowland Circle; 5. Crystal filter and direct radiation block for detector. The spectrometer is adjusted while the source remains at the same position.

The first concern was evidence that the detector material was being activated by ambient light in addition to radiation focused by the crystal. To prevent this, the cassette was coated in a black, absorptive dye through an aluminum anodization process (see Figure 4.2c).

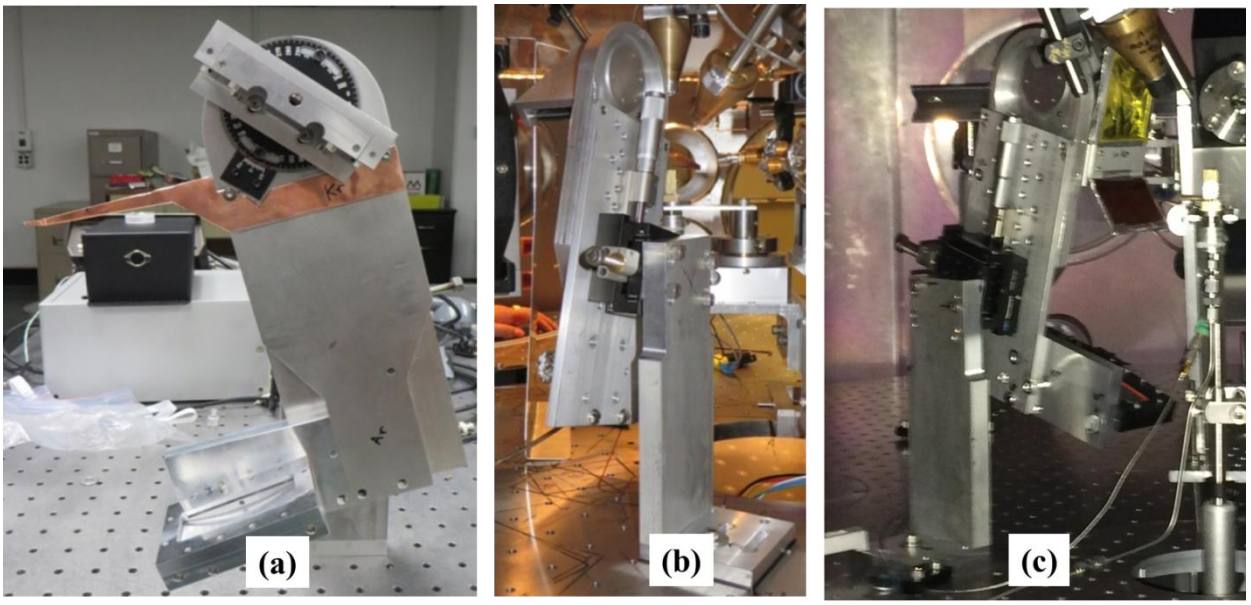

Figure 4.2: Photos of the Johann spectrometer. a. The spectrometer body, crystal holder, and film holder; b. The spectrometer fielded in the Phoenix chamber for experiments on UNR's Leopard laser facility; The spectrometer fielded in the Titan chamber for experiments on LLNL's Titan laser.

The second concern was that direct radiation from the source would reach the detector. Direct radiation would activate the x-ray film along with ambient light and affect the quality of the spectra. The third concern was that excessive radiation or even debris from the source could reach the crystal causing damage. Damaged crystals are not able to provide as high of resolution and are costly to replace. This would be an even greater concern for higher energy radiation sources. To address this issue, three radiation blocks were made, one for each of the spectrometer's observable spectral ranges (object 5 in Figure 4.1). Each radiation block has two areas where filtering materials can be attached. The first area provides a window between the source and crystal where filters can be placed to attenuate the radiation and shield the crystal from debris. The second area provides a surface where dense materials like lead or tungsten could be placed to

completely block direct radiation from reaching the detector. After these changes were made, the spectrometer was tested with 40 J laser-plasma source and the results will be discussed in the next section.

For the selectively reflecting element, the Johann spectrometer uses a Si crystal curved and around a cylindrical surface with a radius of 275 mm. A 7.5 μm Kapton film (>1.4 keV) is used to filter and protect the crystal. The detector used the x-ray sensitive Kodak Biomax MS film. A double 0.15 μm Al coated 3 μm Mylar film is used to filter the detector. The spectrometer can be setup in three different configurations to observe different spectral ranges. These ranges are 3.91-4.58 Å for K-shell Ar ions, 5.26-5.73 Å for L-shell Kr ions, and 2.5-3.14 Å for L-shell Xe ions.

4.3 Tests of Johann Spectrometer with Laser-plasma Sources

The Johann spectrometer was first tested at the Leopard Laser facility (see Figure 4.2b). X-ray spectra were recorded from laser plasma radiation sources created by Ar and Kr gas jets irradiated by the Leopard Laser. The Leopard Laser's short pulse mode was used which provides a 350 fs long pulse of 1.057 μm laser light with an energy of 10-15 J. The x-ray spectra from a Kr gas jet irradiated with a 14.6 J pulse are shown in figure 4.3 (Kantsyrev *et al.* 2016a). A 600 PSI backing pressure was used to generate the gas jet from a linear supersonic nozzle and there was a delay of 1000 μs between triggering the gas valve and triggering the laser. The radiation from Ne-like (Ne) and Na-like (Na) Kr ions was observed. Modeling of the spectra estimated the resolution to be 1200 ($\lambda/\Delta\lambda$).

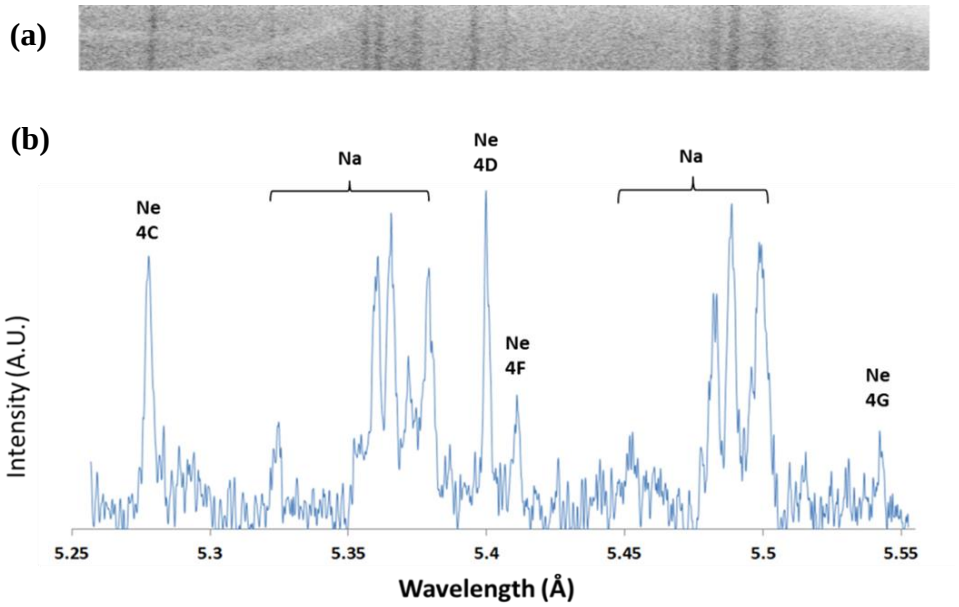

Figure 4.3: X-ray spectrum of Kr obtained with the Johann spectrometer from shot 1300 on the Leopard laser facility. a. film; b. densitogram.

After the modifications were made to the spectrometer to prevent undesirable effects from direct radiation and ambient light, it was tested with the Titan laser at the Jupiter Laser Facility at Lawrence Livermore National Laboratory (Kantysrev *et al.* 2016b). The Titan laser was operated in its second harmonic mode which provides a 0.7 ps pulse of 527 nm laser light with an energy of approximately 40 J. The spectra from a Kr gas jet irradiated by the Titan laser are shown in figure 4.4. The same nozzle, backing pressure, and gas delay time as the previously discussed shot were used. The most intense spectral lines from Ne-like (Ne) and Na-like (Na) Kr ions were identified.

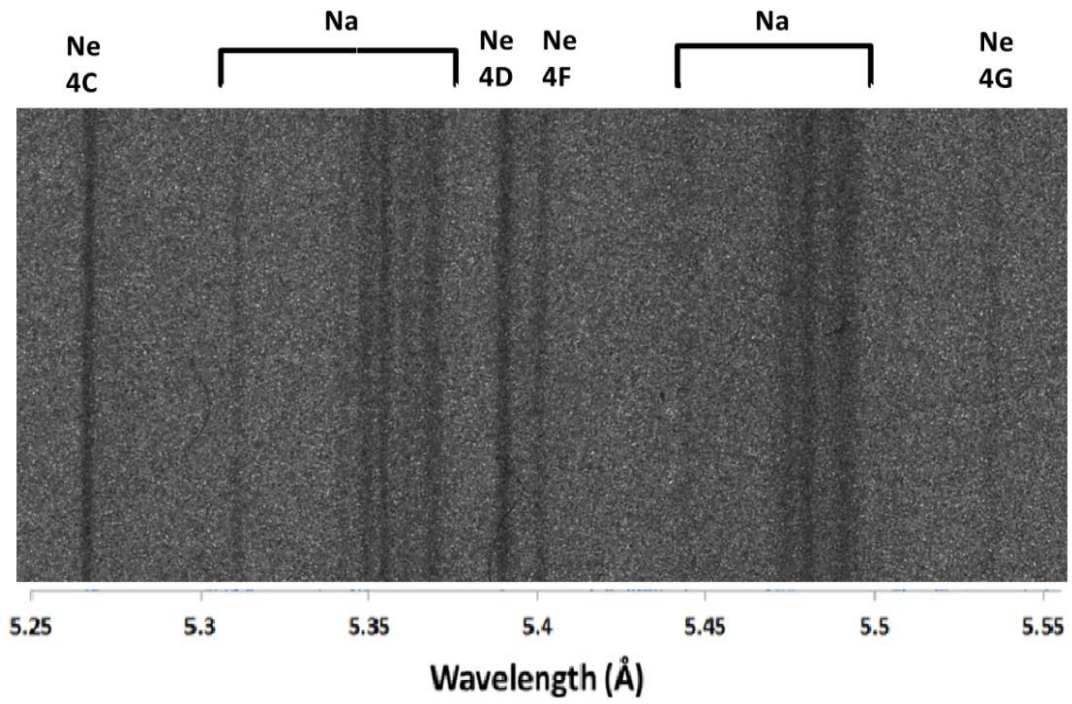

Figure 4.4: X-ray spectrum of Kr obtained with the Johann spectrometer from shot 22 on the Titan Laser.

Chapter 5: Development of Spectropolarimeter

5.1 Motivation

The Johann spectrometer was designed to record specific spectral lines used for determining two important and often measured plasma parameters: electron temperature and density. Two plasma characteristics that have not been extensively measured are the electron distribution function and magnetic field. Measurements of these quantities can provide information about the anisotropy of plasma processes. This information can be gathered through measurements that take advantage of polarization of x-rays on reflection from crystals (see Figure 1.7). A prototype of the spectropolarimeter has previously been used to measure time and spatially integrated polarization-dependent spectra of Ti K-shell ions in x-pinch plasmas imploded at UNR's Nevada Terawatt Facility (Shlyaptseva *et al.* 2001). The relative intensities of Ti He-like and Li-like lines differed between the spectra recorded with dispersion planes perpendicular and parallel to the pinch axis. X-ray pinhole images indicated a strong electron beam in the vertical direction that might explain differences in the ratios of intensities of lines between spectra with different polarization sensitivities. After these initial successful measurements, a new spectropolarimeter was developed for polarization dependent measurements of Mo x-pinch plasmas (see Figure 5.1).

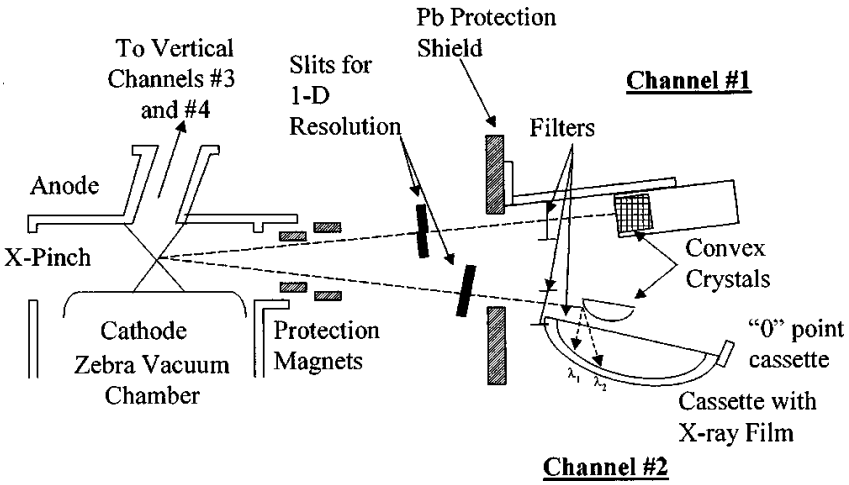

Figure 5.1: Illustration of a spectropolarimeter with one-dimensional resolution setup for the Zebra generator.

There were three main goals of the modifications of this spectropolarimeter. The first goal was to provide 1D spatial resolution of polarization sensitive spectra. The second goal was to improve the precision and ease of alignment. The third goal was to prepare the spectropolarimeter to record L-shell spectra of Mo in two orthogonal polarization directions from Mo x-pinches imploded on UNR's Zebra generator. Modeling of spectra of a Mo plasma with and without the presence of hot electrons can be seen in Figure 5.2 (Shlyaptseva *et al.* 2003). The spectrometer will be used to record experimental data that can be compared to synthetic L-shell Mo spectra and used to investigate polarization dependent properties.

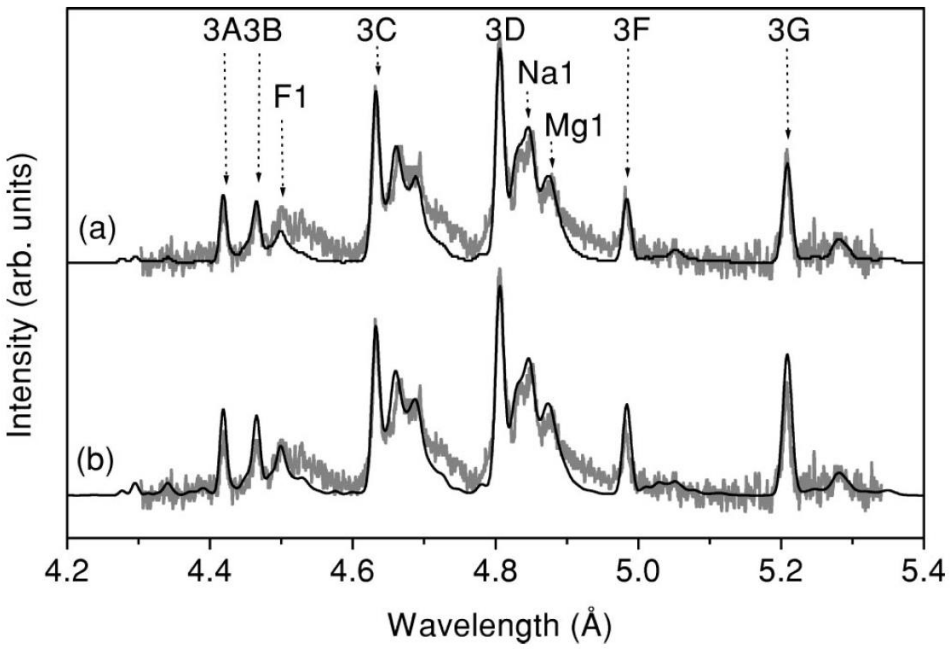

Figure 5.2: L-shell Mo spectra. The gray line is experimental spectrum from a 35.3 μm Mo x-pinch and the black lines are modeled spectrum. a. Mo plasma with no hot electrons, a 1025 eV electron temperature, and a 4×10^{21} cm^{-3} electron density; b. Mo plasma with 5.5% hot electrons, a 750 eV electron temperature, and a 5×10^{21} cm^{-3} electron density (Shlyaptseva *et al.* 2003).

5.2 Design of a Spectropolarimeter with 1D Spatial Resolution

To provide 1D spatial resolution of the plasma source a new chamber was designed to lie between Zebra's discharge chamber and the spectropolarimeter's crystal and detector chamber (see Figure 5.4). Inside this chamber two slits are held on mounts that have fine adjustment in two directions orthogonal to the direction of propagation of radiation. There is one slit for each channel of the spectropolarimeter (objects 2 in figure 5.3). The slit lies between the radiation source and crystal and spacially resolves the image of the source in the direction perpendicular to the length of the slit. For channel 1

in Figure 5.3a, the spectra will provide spatial resolution of the source in the direction along the z-pinch axis. For channel 2 in Figure 5.3b, the spectra will provide spatial resolution of the source in the direction perpendicular to the z-pinch axis. The width of each is slit is 0.5 mm, the distance between the source and each slit is 61 cm, the distance between each slit and crystal is 43 cm, and the distance between each crystal and detector is 13.5 cm. So the minimum spatial resolution due to geometric constraints is about 1 mm, according to equation 5.1:

$$\Delta \boldsymbol{L_{geom}} = \boldsymbol{d}\frac{\boldsymbol{a}+\boldsymbol{b}}{\boldsymbol{b}} \tag{5.1}$$

Where ΔL_{geom} is the resolution due to geometry only, d is the width of the slit, a is the distance from the source to the slit, and b is the distance from the slit to the detector. This will provide enough resolution to observe variation in polarized radiation in the x-pinch plasma in the axial and radial directions.

Certain modifications were made to the spectrometer to aid in alignment and calibration. Adjustability was prioritized in these modifications just like in the design of the Johann spectrometer. The slit and crystal holders were designed to provide at least coarse adjustment in all directions (see Figure 5.4). The slit holders also have fine adjustment in two translational directions and the crystal holders have fine adjustment in two translational and one rotational directions. These features allow the spectrometer to be quickly adusted during alignment. They also allow the spectrometer to be adapted to other crystal types, geometries, and x-ray wavelength ranges. Like the Johann spectrometer, removable clips were made to hold thin films that filter radiation incident on the crystal and the detector was insulated to prevent activation from ambient light.

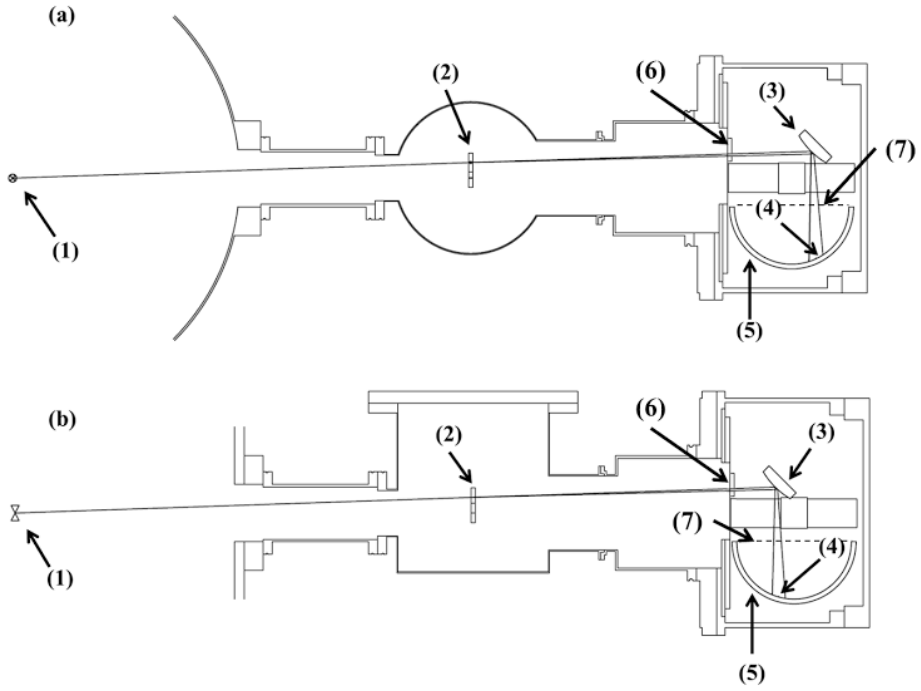

Figure 5.3: Schematic of the modified spectropolarimeter. a. Horizontal cross section of the spectropolarimeter depicting the channel 1 spectrometer; b. Vertical cross section of the spectropolarimeter depicting the channel 2 spectrometer. 1. X-pinch radiation source; 2. Slit; 3. Crystal; 4. Location on detector of polarized radiation; 5. Detector 6. Crystal filters; 7. Detector filters.

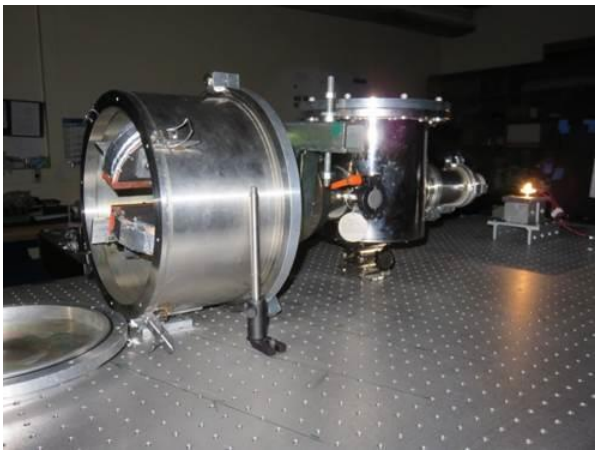

Figure 5.4: Photo of the spectropolarimeter during optical tests.

The spectropolarimeter was developed to record polarization sensitive spectra at many different wavelengths by using different crystals. It has been initially prepared to

record x-ray spectra from L-shell Mo ions at wavelengths near 4.6 Å using two α-quartz crystals with interatomic plane distances of 6.687 Å. This crystal material was chosen so that radiation from 4.6-4.85 Å is selectively reflected from the crystal at a Bragg angle of about 45° for x-ray radiation. At this angle, radiation reflected from the crystal will be polarized in the direction parallel to the surface of the crystal. Each spectrometer channel is rotated 90° from each other with respect to beamline axis. So each recording will consist of a pair spectra that have the same wavelength range but are sensitive to orthogonal directions of polarization of radiation in the range 4.6-4.85 Å. Like the Johann spectrometer, the spectra are recorded on Kodak Biomax MS film. With these adjustments the spectropolarimeter will be used to record 1D resolved, polarization sensitive measurements of important diagnostic lines to characterize the electron distribution function of Mo X-pinch plasmas created on the 1 MA Zebra generator.

Chapter 6: Conclusion

This thesis focused on both the development of a plasma radiation source and instrumentation to make quality, information-rich measurements of plasma parameters in laboratories here at the University of Nevada, Reno and elsewhere. As stated earlier, the general goals of University scale plasma study are: measure and understand plasma radiation and dynamics, support efforts toward Inertial Confinement Fusion, develop radiation sources for x-ray effects testing, x-ray backlighting, or x-ray lasers, create and study laboratory plasmas with properties similar to astrophysical plasmas, calibrate plasma diagnostics, and train future plasma scientists. Several more specific goals were accomplished in the work discussed here.

In chapter two the renovation of a compact z-pinch plasma source was discussed. This included the near doubling of its energy storage capacity from 1.1 kJ to 2.1 kJ, reducing the electrical networks inductance form 20 nH to 7.5 nH, increasing the diagnostic access points from four to six, and improvements to the safety and control system. After these improvements were made, the plasma generator was tested in its vacuum spark operation mode and the peak current achievable at a 17 kV Stinger Bank charge was increased from 40-60 kA to 111 kA. The improved facility has been named Sparky II.

Chapter three discusses the development and characterization of a system to perform gas-puff z-pinch experiments on the Sparky II facility. This system uses a fast valve to inject a jet of gas in to the load area of the machine. The jet is then pre-ionized

and formed into a hollow shell structure when it enters the anode-cathode gap. The Sparky II machine and gas-puff system was made modular so that the machine could be transitioned between vacuum spark mode and gas-puff mode within a day. Interferometry measurements of the gas-jet produced by the system showed that it had an approximately hollow shell like structure which is optimal for long, uniform implosions that can provide a consistent source of radiation.

Chapter four details the development and implementation of a horizontal focusing Johann type x-ray spectrometer. The spectrometer was designed to adapt to several different experimental conditions in order to measure radiation from various plasma sources. The spectrometer has measured K-shell ions from Ar plasmas created at UNR's Leopard Laser Facility and LLNL's Titan Laser allowing plasma conditions to be estimated. The resolution of the spectra was estimated to be about 1200 ($\lambda/\Delta\lambda$) which is more than double the resolution typically achieved with the convex crystal spectrometers used. In the future the spectrometer will be used on the Sparky II facility to record spectra from single shots of the device from either vacuum-spark or gas-puff z-pinches.

Chapter five discusses the development of a spectropolarimeter to make polarization sensitive measurements of z-pinch implosions at UNR's Zebra generator. The spectropolarimeter was designed to simultaneously record two sets of spectra: one sensitive to radiation polarized in the horizontal direction with 1D resolution along the pinch's radial direction and another sensitive to radiation polarized in the vertical direction with 1D resolution along the pinch's z-axis. The device will be used to look for spatial and polarization dependence of radiation from L-shell ions in a Mo x-pinch plasma. This information could be used to assess anisotropy in plasma processes.

I presented the research discussed above at four conferences in two oral talks (Cooper *et al.* 2014b), (Cooper *et al.* 2016), and two posters (Cooper *et al.* 2015a), (Cooper *et al.* 2015b). Results from spectra of Kr gas jet laser-plasmas recorded with the Johann spectrometer were published in two papers which I coauthored (Kantsyrev *et al.* 2016a), (Schultz *et al.* 2016). The development of a code to plan experiments with horizontal focusing spectrometers like the Johann spectrometer discussed above was the subject of a senior thesis done by an undergraduate student whom I mentored (Coleman 2016). I hope that the work presented here will be continued and expanded upon by future physics students who are interested in plasma dynamics and radiation study.

References

M. E. Weller, A. S. Safronova, J. Clementson, V. L. Kantsyrev, U. I. Safronova, P. Beiersdorfer, E. E. Petkov, P.G. Wilcox, and G. C. Osborne, *Extreme ultraviolet spectroscopy and modeling of Cu on the SSPX Spheromak and laser plasma "Sparky",* Review of Scientific Instruments, **83**, 10E101 (2012).

V.L. Kantsyrev, K.A. Schultz, V.V. Shlyaptseva, A.S. Safronova, I.K. Shrestha, G.M. Petrov, J.J. Moschella, E.E. Petkov, A. Stafford, M.C. Cooper, M.E.Weller, W. Cline, P. Wiewior, and O. Chalyy, *Study of x-rays produced from debris-free sources with Ar, Kr and Kr/Ar mixture linear gas jets irradiated by UNR Leopard laser beam with fs and ns pulse duration*, High Energy Density Physics **19**, 11–22 (2016a).

J.L. Giuliani, F.N. Beg, R.M. Gilgenbach, V.L. Kantsyrev, B.R. Kusse, V.V. Ivanov, and R. Presura, *Plasma Pinch Research on University Pulsed-Power Generators in the United States*, IEEE Transactions on Plasma Science, **40**, 3246-3264 (2012).

A. Stafford, A. S.Safronova, V. L.Kantsyrev, S. F.Keim, M. E.Weller, I.Shrestha, and V. V.Shlyaptseva, *Radiation from mid-atomic-number X-pinches at 1.5–1.7 MA*, Physics of Plasmas, **23**, 101209 (2016).

A. Schulz, M. Hebach, F. Walden, F.B. Rosmej and H-J Kunze, *Z-scaling of K-alpha-radiation from micropinches in low-inductance vacuum sparks*, Proceedings on the International Conference on Phenomena in Ionized Gases **1**, 347 (1993).

J.L. Giuliani and R.J. Commisso, *A Review of the Gas-Puff Z-Pinch as an X-Ray and Neutron Source*, IEEE Transactions on Plasma Science, **43**, 2385-2453 (2015).

H. Johann, et al., Z Phys **69**, 185 (1931).

E. Aglitskiy, et al., Preprint FIAN, N**79** (1974).

A. S. Shlyaptseva, S. B. Hansen, V. L. Kantsyrev, B. S. Bauer, D. A. Fedin, N. Ouart, S. A. Kazantsev, A. G. Petrashen, and U. I. Safronova, *X-ray spectropolarimetry of high-temperature plasmas*, Review of Scientific Instruments **72**, 1241 (2001).

D. Brewster, *On the laws which regulate the polarisation of light by reflection from transparent bodies*, Philosophical Transactions of the Royal Society of London, **105**, 125-159 (1815).

V. Kantsyrev, D. Fedin, M. Savage, W. Cline, V. Nalajala, S. Pokala, I. Shrestha, *Table-top z-pinch and laser-plasma x-ray/EUV facility "Sparky"*, SPIE Conference Proceedings, 59180-59186 (2004).

M.C. Cooper, *Renovation of the Compact Z-pinch Facility "Sparky" and Development and Tests of Focusing Crystal X-ray Spectrometers*, Senior Thesis, University of Nevada, Reno (2014a).

R.A. Serway and J.W. Jewett, *Physics for Scientists and Engineers with Modern Physics*, 9th ed., Brooks/Cole (2014).

M. Kiefer, K. Shaw, K. Struve, and M. Widner, *SCREAMER User's Guide for Version 2.2*, Sandia Corporation (1999).

V. Nalajala, *Data Acquisition, Control and Analysis of Optical Signal of Compact Z-pinch Plasma Machine*, Master's Thesis, University of Nevada, Reno (2004).

L. Alfredo, CC BY-SA 4.0, (https://en.wikipedia.org/wiki/Rogowski_coil#/media/File: Rogowsky_coil.png), (2011).

L.A. Kojovic, R. Beresh, M.T. Bishop, R. Javora, B. Magruder, P. McLaren, B. Mugalian, and A. Offner, *Practical Aspects of Rogowoski Coil Applications to Relaying*, IEEE PSRC Special Report (2010).

A.K. Zver'kov, V.L. Kantsyrev, A.A. Krivtsov, and A.S. Shlyaptseva, *X-ray emission from a "plasma point" source. Effects of the atomic number of the anode material and the capacitor voltage*, Sov. Phys. Tech. Phys. **31**, 595-597 (1986).

V.L. Kantsyrev, K.I. Kopytok, and A.S. Shlyaptseva, *Results of the study of the new type of compact gas-puff plasma source of SXR (soft x-ray),* Proceedings of the 3rd International Conference on Dense Z-pinches, London, United Kingdom (1994).

M.A. Lieberman, A.J. Lichtenberg, *Principles of plasma discharges and materials processing,* Wiley-Interscience (2005).

K. Krishnavedala, CC BY-SA 4.0 (https://en.wikipedia.org/wiki/Paschen%27s_law#/ media/File:Paschen_curves.svg), (2014).

J.J. Moschella and V.L. Kantysrev, *Laser Generated X-rays in an Underdense Plasma Produced in a High-Density Linear Gas Jet*, HDTRA1-11-0011 Annual Report, **2**, 1-22 (2012).

V.L. Kantsyrev, K.A. Schultz, V.V. Shlyaptseva, A.S. Safronova, M.C. Cooper, I.K. Shrestha, E.E. Petkov, A. Stafford, J.J. Moschella, M.T. Schmidt-Petersen, C.J. Butcher, G.E. Kemp, S.D. Andrews, and K.B. Fournier, *Study of laser-generated debris free x-ray sources produced in a high-density linear Ar, Kr, Xe, Kr/Ar and Xe/Kr/Ar mixtures gas jets by 2w, sub-ps LLNL Titan laser*, The 58th Annual Meeting of the APS Division of Plasma Physics, San Jose, CA, USA, October 31-November 4 (2016b).

A.S. Shlyaptseva, S.B. Hansen, V.L. Kantsyrev, D.A. Fedin, and N. Ouart, *Advanced spectroscopic analysis of 0.8—1.0-MA Mo x pinches and the influence of plasma electron beams on L-shell spectra of Mo ions*, Physical Review E **67**, 026409 (2003)

M.C. Cooper, V.L. Kantsyrev, A.S. Safronova, I.K. Shrestha, K.A. Schultz, V.V. Shlyaptseva, M.E. Weller, A. Stafford, E.E. Petkov, M.T. Schmidt-Petersen, M.Y. Lorance, W. Cline, C. Davidson, *Renovation of the Compact Z-pinch Facility "Sparky" and Development and Tests of Focusing Crystal X-ray Spectrometers*, Annual APS Meeting of the Far West Section, Reno, NV, October 24-25 (2014b).

M.C. Cooper, V.L. Kantsyrev, A.S. Safronova, I.K. Shrestha, V.V. Shlyaptseva, K.A. Schultz, E.E. Petkov, W. Cline, and C. Davidson, *X-ray spectrometer and spectropolarimeter for the study of high temperature and density laboratory plasmas*, The 2016 Annual Meeting of the Far West Section of The American Physical Society, Davis, CA, October 28-29 (2016).

M.C. Cooper, V.L. Kantsyrev, A.S. Safronova, I.K. Shrestha, V.V. Shlyaptseva, K.A. Schultz, M.E. Weller, A. Stafford, E.E. Petkov, M.T. Schmidt-Petersen, W. Cline, C. Davidson, *Improvements to the Compact Z-pinch Facility "Sparky" and Development and Applications of Focusing Crystal X-ray Spectrometers*, 3rd International Workshop on Radiation from High Energy Density Plasmas (RHEDP), South Lake Tahoe, June 9-12 (2015a).

M.C. Cooper, V.L. Kantsyrev, A.S. Safronova, I.K. Shrestha, V.V. Shlyaptseva, K.A. Schultz, A. Stafford, E.E. Petkov, M.T. Schmidt-Petersen, W. Cline, and C. Davidson, *Renovating "Sparky" Facility to Investigate Gas-puff Z-pinches with X-ray Focusing Spectrometers*, The 2015 Annual Meeting of the Far West Section of the American Physical Society, Long Beach, CA, October 29-31 (2015b).

K.A. Schultz, V.L. Kantysrev, A.S. Safronova, J.J. Moschella, P. Wiewior, V.V. Shlyaptseva, M.E. Weller, E.E. Petkov, I.K. Shrestha, A. Stafford, and M.C. Cooper, *Characterization of pure and mixed Ar, Kr, and Xe gas jets generated by different nozzles and a study of x-ray radiation yields after interaction with a sub-ps laser pulse,* Physics of Plasmas **23**, 101207 (2016).

T.S. Coleman, *A computer application to aid in the use and modification of a Johann type x-ray spectrometer in hot dense plasma experiments*, Senior Thesis, University of Nevada, Reno (2016).